Atmos. Chem. Phys. Discuss., 10, 27015–27074, 2010
www.atmos-chem-phys-discuss.net/10/27015/2010/
doi:10.5194/acpd-10-27015-2010

Atmospheric Chemistry and Physics Discussions

Synergetic monitoring of Saharan dust plumes and potential impact on surface: a case study of dust transport from Canary Islands to Iberian Peninsula

C. Córdoba-Jabonero[1], M. Sorribas[1], J. L. Guerrero-Rascado[2,*], J. A. Adame[1], Y. Hernández[3], H. Lyamani[2], V. Cachorro[4], M. Gil[1], L. Alados-Arboledas[2], E. Cuevas[3], and B. de la Morena[1]

[1]Instituto Nacional de Técnica Aeroespacial (INTA), Atmospheric Research and Instrumentation Branch, Torrejón de Ardoz (Madrid), Spain
[2]Universidad de Granada (UGR), Andalusian Environmental Centre (CEAMA), Group of Atmospheric Physics, Granada, Spain
[3]Agencia Estatal de Meteorología (AEMET), Atmospheric Research Centre of Izaña, Sta. Cruz de Tenerife, Spain
[4]Universidad de Valladolid (UVA), Group of Atmospheric Optics, Valladolid, Spain

[*]now at: Évora Geophysics Centre (CGE), University of Évora, Évora, Portugal

Received: 14 July 2010 – Accepted: 13 October 2010 – Published: 9 November 2010

Correspondence to: C. Cordoba-Jabonero (cordobajc@inta.es)

Discussion Paper | Discussion Paper | Discussion Paper | Discussion Paper |

Abstract

Synergetic use of meteorological information, remote sensing both ground-based active (lidar) and passive (sun-photometry) techniques together with backtrajectory analysis and in situ measurements is carried out for the characterization of dust intrusions. A case study of air masses advected from Saharan region to the Canary Islands and the Iberian Peninsula, relatively located close and far away from the dust sources, respectively, was monitored from 11 to 19 March 2008. The observations were performed over three Spanish geographically strategic within the dust-influenced area stations along a common dust plume pathway. A 4-day long dust event (13–16 March) over the Santa Cruz de Tenerife Observatory (SCO), and a linked short 1-day dust episode (14 March) in the Southern Iberian Peninsula over both the Atmospheric Sounding Station "El Arenosillo" (ARN) and the Granada station (GRA) were detected. Meteorological situation favoured the dust plume transport over the area under study. Backtrajectory analysis clearly showed the Saharan origin of the dust intrusion. Under the Saharan air masses influence, AERONET Aerosol Optical Depth at 500 nm (AOD^{500}) ranged from 0.3 to 0.6 and Angstrom Exponent at 440/675 nm wavelength pair ($AE^{440/675}$) was lower than 0.5, indicating a high loading and predominance of coarse particles during those dusty events. Lidar observations characterized their vertical layering structure, identifying different aerosol contributions depending on altitude. In particular, the 3-km height layer observed over ARN and GRA stations corresponds to that dust plume transported from Saharan region after crossing through Canary Islands at 3 km height as observed over SCO site as well. No significant differences were found in the lidar (extinction-to-backscatter) ratio (LR) estimation for that dust plume over all stations when a suitable aerosol scenario for lidar data retrieval is selected. Lidar-retrieved LR values of 65–70 sr were obtained during the principal dusty episodes. These similar LR values found in all the stations suggest that dust properties were kept unchanged in the course of its medium-range transport. In addition, the potential impact on surface of that Saharan dust intrusion over the Iberian Peninsula was evaluated by ground-level

in situ measurements for particle deposition assessment together with backtrajectory analysis. However, no connection between those dust plumes and the particle sedimentation registered at ground level is found. Differences on particle deposition process observed in both Southern Iberian Peninsula sites are due to the particular dust transport pattern occurred in each station.

1 Introduction

The important role that suspended matter plays in the radiative balance of the atmosphere is widely known, influencing both solar and thermal radiation. Evaluation of this aerosol-radiation interaction is essential for climate forcing assessment at both local and regional scales. However, large uncertainties exist at present caused in particular by an incomplete characterization of the optical, microphysical and chemical properties of the aerosols (IPCC, 2007).

Desert dust represents about 40% of aerosol loading yearly injected into the troposphere (Andreade, 1995). One half of this amount is attributed to the Saharan desert. Since 2001, different studies have reported more precise dust emission estimates ranging from 1000 to 2150 Tg yr^{-1} (see the review work of Zender et al., 2004, and references therein). Once suspended, the dust particles can be transported by strong winds at medium- and long-range distances (Hamonou et al., 1999; Ansmann et al., 2003). In the course of that transport, the atmospheric impact of dust can be different, since physical and chemical transformations can occur, affecting both the optical and microphysical properties of dust.

Dust particles lifted by outbreaks in the Saharan region can travel very long distances and reach Europe and Mediterranean areas, and even after crossing the North Atlantic Ocean, reach the Southeastern United States (Prospero, 1999; Prospero et al., 2002). In particular, a long-range dust transport characterization during the SAMUM 2006 campaign in North Africa area with dust plumes crossing towards South Europe has been recently reported (Müller et al., 2009) for transport modelling validation. In that

work, EARLINET (European Aerosol Research LIdar NETwork, http://www.earlinet.org) observations together with both AERONET (AErosol RObotic NETwork, http://aeronet.gsfc.nasa.gov) data and backtrajectory analysis, among others, have been used for that purpose. At the same time, Mediterranean studies are being carried out in order to assess the potential impact of the dust in the chemical processes occurring over that influenced area by using the same kind of instrumentation (Balis et al., 2000; Dulac et al., 2009).

These studies reflect the importance of the synergetic use of both remote sensing from ground-based and satellite platforms and in situ observations for the characterization of the vertical and horizontal distribution of dust. Height-resolved information of the dust properties is crucial for the understanding of the aerosol-ozone-UV interactions (i.e., Balis et al., 2002; Zerefos et al., 2002; Bonasoni et al., 2004), and even for both aerosol forecast modelling (i.e., Perez et al., 2006) and satellite data evaluations (i.e., Pappalardo et al., 2010). On the other hand, the dust impact on surface is getting more and more important in diverse socio-economic aspects and health issues (WMO, 2003).

A case study of medium-range dust transport from Saharan region as monitored crossing the Canary Islands and advected to the Iberian Peninsula is shown in this study. Canary Islands present a singular location due to their close proximity to Saharan dust sources, acting as a first-detection site for fresh-dust observations. Iberian Peninsula represents the observational environment for potential transformation monitoring of those dust plumes, as transported far away from those source regions. Several studies leading to characterize dust intrusions reaching these dust-influenced areas have been previously performed by using different aerosol active and passive techniques, modelling methods and air quality methodologies, including ground-based and satellite platforms (Müller et al., 2003; Lyamani et al., 2005; Perez et al., 2006; Escudero et al., 2007; Toledano et al., 2007a,b; Cachorro et al., 2008; Guerrero-Rascado et al., 2008, 2009; Querol et al., 2008; Basart et al., 2009; Tesche et al., 2009). In this work we intend to extend that kind of dust characterization along the path as based

on both the potential changes of the dust properties in the course of the same plume travelling and its impact on surface deposition.

The aim of this work is focused on the monitoring of a dust plume, regarding both vertical structure and physical/optical features, coming from Saharan region and its potential surface deposition by using lidar, sun-photometry and surface in situ measurements in three Spanish strategic stations deployed along the same path of this dust plume: the subtropical Santa Cruz de Tenerife Observatory (SCO-AEMET), around 1000 km far from the Saharan dust sources, and two sites located in the South of the Iberian Peninsula: the Atmospheric Sounding Station "El Arenosillo" (ARN-INTA), and the Granada station (GRA-UGR), placed at around 1350 km and 1600 km, respectively, from Canary Islands. A dust event sequentially covering all three stations on March 2008 was monitored and analyzed. Synergetic use of AERONET columnar-integrated data for dust intrusion evidence and meteorological synoptic situation together with backtrajectory analysis for dust plume tracking completes this study.

Description of the measurements sites and methodology used in this work are detailed in Sects. 2 and 3, respectively. A meteorological overview for the monitored period is shown in Sect. 4. Section 5 presents results and discussion. Main conclusions are exposed in Sect. 6.

2 Measurement sites

Three Spanish geographically strategic within the dust-influenced area stations have been chosen for this study in relation to their lidar, sun-photometry and surface in situ measurement capabilities. The relative position of these three sites respect to Saharan region is shown in Fig. 1.

2.1 Santa Cruz de Tenerife Observatory (SCO-AEMET)

The Santa Cruz de Tenerife Observatory (SCO) is a subtropical station (28.5° N 16.2° W, 52 m a.s.l.), a coastal urban background site located in Tenerife (Canary Islands). SCO station is managed by the Atmospheric Research Centre of Izaña of the Spanish Agency of Meteorology (AEMET). This station is both a NASA/AERONET and NASA/MPLNET (MicroPulse Lidar NETwork, http://mplnet.gsfc.nasa.gov) site, and belongs to the recently formed Spanish and Portuguese Aerosol Lidar NETwork (SPALINET, http://www.lidar.es/spalinet/). It is a multi-instrumented station devoted to atmospheric research focused on both trace gases and particles measurements by using in situ techniques and meteorological monitoring in continuous operation. Remote sensing techniques (lidar, sun-photometry) are also used to complement the aerosol measurement program at SCO site. This station has an excellent location and qualities for different atmospheric phenomena studies.

Dust research has been performed over SCO station by using both AERONET columnar-integrated data and different surface in situ measurements for air quality assessment. Results indicate that the mineral dust dominates the aerosol regime as a consequence of frequent Saharan dust outbreaks (Basart et al., 2009). $PM_{10}/PM_{2.5}$ (Particulate Monitor for aerosols less than 10 and 2.5 µm size, respectively) concentrations found during African dust outbreaks were higher in SCO than other Spanish stations due to its closer proximity to African desert source regions (Querol et al., 2008).

2.2 Atmospheric Sounding Station "El Arenosillo" (ARN-INTA)

The Atmospheric Sounding Station "El Arenosillo" (ARN) belongs to National Institute for Aerospace Technology (INTA) and is located at the Southwest of the Iberian Peninsula (37.1° N 6.7° W, 40 m a.s.l.). ARN is an NASA/AERONET site; it is a multi-instrumented station dedicated to atmospheric research by in situ and remote sensing techniques. "El Arenosillo" observatory is located in a rural protected environment, near the Doñana National Park, and at less than 1 km far from the Atlantic coastline.

The station has an exceptional situation for first dust detection once crossing over the Southwestern Iberian Peninsula.

Dust research over this station has been focused on both AERONET columnar-integrated and surface in situ measurements. Previously reported AERONET data for desert dust events over this site indicate high turbidity and a predominance of coarse particles (Toledano et al., 2007a,b). In addition, desert dust air masses presented a relevant annual frequency of 18% with a mean duration period of 4 days, and they were more frequent in February/March and summer months (Prats et al., 2008; Toledano et al., 2009). The strongest North African desert dust intrusion over the Iberian Peninsula was also analyzed over this site (Cachorro et al., 2008). Surface in situ measurements during 2004 summertime show relevant absorption coefficients (Mogo et al., 2005) and main PM_{10} sources were regional, crustal, industrial and marine (Gonzalez-Castanedo et al., 2008). Analysis of the sub-micrometer particle number size distribution under different aerosol-type occurrence shows a predominance of accumulation mode particles for desert dust aerosol with a modal diameter around 0.1 µm (Sorribas, 2008). ARN is a representative rural background site in the Iberian Peninsula, where desert dust intrusions are relatively frequent.

2.3 Granada station (GRA-UGR)

Granada station (GRA) is a non-industrialized urban observatory placed in a natural basin surrounded by mountains with the highest mountain range located to the Southeast (with altitudes above 3000 m). It is managed by the Andalusian Environmental Centre (CEAMA) of the University of Granada (UGR). GRA site is both a NASA/AERONET and EARLINET station, and is also included in SPALINET like SCO site. Its multi-instrumental capabilities, including active and passive remote sensing and in situ measurements, allow for monitoring and characterizing a wide array of atmospheric parameters. This station is located at the same latitude than ARN, but far from the Atlantic coast at the Southeast of the Iberian Peninsula (37.2° N 3.6° W), about 50 km from the Western Mediterranean coast and at higher altitude (680 m a.s.l.)

than the other measurement sites involved in this study.

Atmospheric aerosol columnar properties have been characterized over Granada (Alados-Arboledas et al., 2003) and specially Saharan dust aerosol features and its variability have already been studied in recent years by using both ground-based sun-photometer and lidar data (Lyamani et al., 2004, 2005, 2006a,b, 2008; Alados-Arboledas et al., 2008; Guerrero-Rascado et al., 2008). Recently Guerrero-Rascado et al. (2009) reported the most extreme Saharan dust outbreak over the Southeastern Iberian Peninsula from different measurements (active/passive and ground-based/satellite), revealing the importance of performing multi-instrumental measurements to properly characterize the contribution of different aerosol types from different sources during extreme events. In addition, aerosol research has also been completed with surface in situ measurements (i.e., Lyamani et al., 2008, 2010), where results indicate that the particle properties follow a clear diurnal pattern with two local maxima occurring in early morning and late evening, as caused by local conditions.

3 Methodology

Height-resolved measurements are carried out by using ground-based aerosol lidars for vertical assessment of the dust intrusion over all three sites. Size-resolved and optical measurements are performed by surface in situ instrumentation for dust impact evaluation on surface once over the Iberian Peninsula. Sun-photometry data and air mass backtrajectory analysis are also included in this study.

3.1 Ground-based lidars: height-resolved measurements

A detailed description of the three aerosol lidars used in this work and their data processing is presented. Main characteristics of them are shown in Table 1. Good results were obtained from a lidar intercomparison on instrument performance and data retrieval algorithms of both the SCO and GRA systems previously performed in the frame

of SPALINET (Sicard et al., 2009). ARN system was tested against the Koldewey Aerosol Raman Lidar (KARL) managed by the Alfred-Wegener Institute (AWI, Germany) and devoted to long-term Arctic aerosol observations obtaining a good agreement on instrument performance (Cordoba-Jabonero et al., 2009).

3.1.1 SCO and ARN systems

Two INTA Micropulse Lidars (MPL), MPL-3 (SES Inc., USA) and MPL-4 (Sigma Space Corp., USA) systems as patented by NASA, were deployed at SCO and ARN, respectively, for dust monitoring over these sites. MPL-3 system is the standard micropulse lidar currently in operation within NASA/MPLNET. An improved version of it, the MPL-4 system, was temporarily installed at ARN in November 2007 to carry out complementary measurements on aerosol monitoring and research. MPL is a robust system with high-pulsed (2500 Hz) and low-energy (7–10 μJ, maximal) "eye-safe" Nd:YLF laser at 523 nm (MPL-3) and 527 nm (MPL-4), operational in full-time continuous mode (24 h a day/365 days a year). These features make available both the temporal and vertical evolution of the dust layering structure with a good resolution.

Lidar backscattered signal is registered in 1-min integrated time and with a vertical resolution of 75 m, as for MPLNET requirements. Raw signal is corrected by several factors affecting the instrument (Campbell et al., 2002). Corrected profiles are hourly averaged in order to increase the signal-to-noise (s/n) ratio.

3.1.2 GRA system

The Raman lidar model LR331D400 (Raymetrics S.A., Greece) is a robust system configured in a monostatic biaxial alignment, pointing vertically to the zenith. It is based on a pulsed Nd:YAG laser with fundamental emission at 1064 nm, and additional emissions at 532 and 355 nm by using second and third harmonic generators. Output energies are 110, 65 and 60 mJ at 1064, 532 and 355 nm, respectively, and pulses of 7 to 9 ns can be fired with a pulse repetition frequency (PRF) of 1, 2, 5 and 10 Hz (a PRF

of 10 Hz has been used in this study). The receiving system consists of a Cassegrain telescope and a wavelength separation unit with dichroic mirrors, interferential filters and a polarization cube, that discriminates seven channels corresponding to elastic wavelengths (1064, 532 parallel-polarized, 532 perpendicular-polarized, and 355 nm), and to nitrogen and water vapor Raman-shifted wavelengths (387, 408, and 607 nm). Raman signals are only used for night-time retrievals. Lidar backscattered signal is registered in 1-min integrated time and with a vertical resolution of 7.5 m.

3.1.3 Lidar data processing

A Klett-Fernald-Sasano iterative inversion algorithm (Fernald et al., 1972; Klett, 1981; Fernald, 1984; Sasano and Nakane, 1984; Klett, 1985; Sasano et al., 1985) is used to retrieve the height-resolved aerosol backscattering coefficient (molecular backscattering coefficients are obtained from local radiosoundings, if available). AERONET Aerosol Optical Depth (AOD) is used to constraint the algorithm convergence, estimating thus the lidar ratio (LR, extinction-to-backscatter ratio). Once this value is determined, the corresponding extinction coefficients can be retrieved, and an hourly-integrated AOD is calculated from day- and night-time measurements.

3.2 Surface in situ instrumentation: size-resolved measurements

Both ARN and GRA sites have similar instrumentation for characterizing surface in situ aerosol particle properties. Particles in the micrometer (0.5–10.0 µm) size range were monitored with an Aerodynamic Particle Size (APS) Spectrometer (TSI Mod. 3321) in both stations. This instrument is a time-of-flight spectrometer that measures the velocity of particles in an accelerating air flow though a nozzle (Holm et al., 1997). For conversion of the micrometer particle number size distribution to the volume-metric one, spherical particles with an effective particle density of 2.0 g cm^{-3} are assumed by using the algorithm as described by Sioutas et al. (1999). Stokes corrections are also applied (Wang and Walter, 1987). In addition, an integrating nephelometer (TSI

Mod. 3563), backscatter shutter included, was used for scattering and backscattering particle properties measurements by splitting the scattered light into blue (450 nm), green (550 nm) and red (700 nm) wavelengths. Thus, an additional Angstrom exponent (AE_{np}) can be inferred from these nephelometer measurements. Other parameter to be examined is the fraction of backscattered light at 550 nm (backscatter fraction, BSC^{550}), defined as the ratio of the integral of the volume scattering function over the backward half solid angle divided by the same one over the full solid angle. Truncation and angular scattering corrections were applied (Anderson and Ogren, 1998).

Dry ambient sub-micrometer size distributions were monitored only in ARN site by using a Scanning Mobility Particle Sizer (SMPS) (Electrostatic Classifier TSI Mod. 3080 and a Condensation Particle Counter TSI Mod. 3022A). This particle spectrometer uses the relation between the particle mobility and the diameter to calculate the particle size (Knutson and Whitby, 1975). Data were obtained in the size range of 14.5–604 nm by using rates of 0.3 and 3.0 l min^{-1} for aerosol and sheath flows, respectively. Volume size distribution for sub-micrometer aerosols was calculated by assuming spherical particles. Datasets were also corrected for losses caused by diffusion processes inside of the instrument (Willeke and Baron, 1993).

3.3 AERONET data: columnar-integrated measurements

All three stations are AERONET sites, routinely performing ground-based aerosol monitoring to assess optical and microphysical properties of the suspended particles. Columnar-integrated data are used for dust intrusion evidence. AERONET inversion products (Dubovik and King, 2000; Dubovik et al., 2006) of level 1.5 (Cloud Screened) are used in this work. Main AERONET parameters used to evidence the dust signature are the Aerosol Optical Depth (AOD) and the Angstrom Exponent (AE): high AOD and low (even close to zero) AE values indicate the presence of dust (large particles) representing dusty conditions over the observational site (Lyamani et al., 2005; Perez et al., 2006; Toledano et al., 2007a,b; Cachorro et al., 2008; Guerrero-Rascado et al.,

2009; Basart et al., 2009). Other retrievals like the single scattering albedo (SSA) and phase function at 180° ($P_{180°}$) are taken into account to derive a columnar-integrated LR ($LR^{AERONET}$) according to the expression (Welton et al., 2002):

$$LR^{AERONET} = 4\pi/SSA \times P_{180°} \quad (1)$$

These $LR^{AERONET}$ values are considered for lidar ratio evaluation in comparison with those estimated by using lidar retrieval algorithms. Unfortunately, AERONET particle size distribution inversions are unavailable for that dusty period, preventing thus the comparison with surface in situ size-resolved concentration measurements.

Spectrally resolved AOD, AE and those other optical parameters (SSA and $P_{180°}$) are derived at visible wavelengths close to the lidar laser wavelength (523–532 nm), depending on the spectral availability for each station. AOD at 500 nm is the one selected if available; otherwise the Angstrom formulation (Angstrom, 1964) is used to derive it. The AE for the 440/675 nm wavelength pair ($AE^{440/675}$) is taken and mean SSA and $P_{180°}$ values between those at 440 and 675 nm is obtained for $LR^{AERONET}$ calculations.

In particular, the criteria adopted for dust event evidence are based on: 1) AOD^{500} values, representing thus a low (AOD^{500}<0.15), moderate (0.15<AOD^{500}<0.35) and high (AOD^{500}>0.35) dust loading over the station; and 2) a threshold $AE^{440/675}$ value <0.5 for dust identification. In this sense, two principal aerosol atmospheric scenarios have been selected according to the following AOD^{500} and $AE^{440/675}$ values: no-dusty conditions with low AOD^{500} and $AE^{440/675}$>0.5 and dusty conditions corresponding to moderate and high AOD^{500} and $AE^{440/675}$<0.5.

3.4 Air mass backtrajectory analysis

Backtrajectories are calculated to determine the origin and the pathway of the air masses affecting the three stations involved in this study. Backtrajectory analysis is performed by using the Hybrid Single Particle Lagrangian Integrated Trajectory (HYSPLIT)

model Version 4 developed by the NOAA's Air Resources Laboratory (ARL) (Draxler and Hess, 1998; Draxler et al., 2009). GDAS (Global Data Analysis System) meteorological files generated and maintained by ARL are used as data input. Kinematical three dimensional backtrajectories are calculated using the vertical wind component given by the meteorological model (Stohl, 1998). In particular, the dust intrusions observed over each station can be thus potentially associated to Saharan sources by examining the HYSPLIT 5-day air mass backtrajectories for each one of three stations (SCO, ARN and GRA). In order to understand the behaviour of the air masses circulating in the boundary layer (BL) and the free troposphere (FT), backtrajectories at three different altitudes above ground level (a.g.l.) have been calculated: 500 m (near the surface), 1500 m (representative of the BL top) and 3000 m (characteristic for FT heights).

4 Meteorological overview

Meteorological situation is examined to explain the synoptic conditions that originate those aerosol scenarios. Synoptic charts are provided by the NOAA/ESRL Physical Sciences Division from their website at http://www.esrl.noaa.gov/psd/ (Kalnay et al., 1996). Selected pictures at three geopotential heights: 700 hPa (around 3000 m a.s.l.), 850 hPa (1500 m a.s.l.) and 925 hPa (800 m a.s.l.), for three different dates as representative of both no-dusty and dusty conditions depending on each station are shown in Fig. 2.

Meteorological conditions on 11 March are characterised by an Atlantic high pressure system centred over the North Atlantic, between the Azores Islands and the Canary Islands, a low pressure system over Mauritania at 700 hPa (around 3000 m a.s.l.), and an enhanced Azores High system shifted eastwards at 850 hPa (1500 m a.s.l.) and 925 hPa (800 m a.s.l.) (see Fig. 2). This situation favours the arrival of Atlantic air masses from Northwestern and Western directions to both ARN and GRA stations. Nevertheless, Atlantic air masses arrive at SCO station by different pathways, in this

case from Northeastern direction (see Fig. 2). Next day (12 March) the synoptic situation is very similar. Air masses have the same origin but with a major influence from Western direction to ARN and GRA areas. In the case of SCO site, air masses arrive from Northeastern direction but with a pathway very close to the Africa coastline.

On 13 March a strong Atlantic high pressure system is well identified over Northern Africa at 700 hPa, extending over the Iberian Peninsula at 850 hPa and 950 hPa. This synoptic situation favours a Southwestern flow over ARE and GRA sites, while SCO site is directly affected by air masses arriving directly from African continent.

Synoptic meteorology on 14 March is determined by a high pressure system centred over Mali at 700 hPa and over Algeria and Libya at 850 hPa and 925 hPa, respectively. This configuration causes the arrival of air masses from Africa continent at the three altitude levels considered and over all the three stations (see Fig. 2). However, the air masses arriving at SCO site have their origin at similar latitudes to the Canary Islands (over the Western Sahara) while the Saharan air masses reaching both ARN and GRA stations have their origin at higher latitudes of the African continent.

Next day (15 March) a change in the synoptic conditions respect to previous days is observed. The Western flow affecting both ARE and GRA sites is completely disconnected from air masses over the Canary Islands which are still originated over the Saharan region. Therefore, dust levels over SCO station would remain high whereas those observed over ARN and GRA sites would decrease, as confirmed by results exposed in the following sections. The situation is similar on 16 March.

On 17–19 March a reinforced Western flow is observed over both ARE and GRA sites at all altitude levels. Regarding SCO station, a change in the synoptic maps is registered for this period. The high system at 700 hPa over Mauritania slowly moves westwards, the Azores high system is observed at its normal position at 925 hPa while a low pressure system over the Northwestern Iberian Peninsula is moving to the South. This meteorological scenario produces a meridional flow over the Canary Islands resulting in a sharp decrease of dust content over SCO.

In summary, the meteorological situation provides optimal conditions for dust intrusion occurrence over the geographical area under study during the analyzed period.

5 Results and discussion

A case study of the medium-range scale transport monitoring of a dust plume describing an Atlantic arch and passing progressively over three Spanish stations is carried out in this work. Synergetic use of lidar observations and surface in situ measurements together with AERONET data retrievals and HYSPLIT backtrajectory analysis is performed for evaluation of the potential changes occurred in the optical and microphysical properties of that dust plume. Dust particle deposition impact on surface once it arrives at and cross the Southern Iberian Peninsula is also examined.

5.1 Saharan dust intrusion identification

5.1.1 Evidence of dust signature

The dust event has been monitored from 11–16 March 2008 over all three stations. According to the dusty conditions criteria adopted (AOD^{500}>0.15 and $AE^{440/675}$<0.5, see Sect. 3.3), a 4-day long dust event (13–16 March) over SCO site and a linked short 1-day dust episode (14 March) over both ARN and GRA stations are found. Daily mean AOD^{500} and $AE^{440/675}$ for these three stations are shown in Fig. 3a,b, respectively (dusty periods are marked by light- and dark-shaded areas over SCO and ARN/GRA sites, respectively).

High (13–14 March) and moderate (15–16 March) AOD^{500} values (see Fig. 3) are found over SCO site (dust event lasts 4 days). In the case of ARN and GRA sites, the dust event lasts only 1 day (14 March). No-dusty conditions with low AOD^{500} (<0.15) and high $AE^{440/675}$ (>0.5) values are observed just before and after this dusty monitored period in each station. These AOD^{500} and $AE^{440/675}$ values together with

AERONET-derived columnar-integrated $LR^{AERONET}$ (see Eq. 1) are also shown in Table 2 for each station. Therefore, AERONET data confirm the dust intrusion signature: high (>0.35)/low (<0.15) AOD^{500} together with low (<0.5)/high (>0.5) $AE^{440/675}$ values are found for those dusty/no-dusty days over all three stations.

5.1.2 Medium-range transport tracking of dust plumes

The origin and pathways of those dust plumes as identified over SCO site and later on ARN and GRA stations are examined by backtrajectory analysis. Five-day air mass backtrajectories are calculated by using HYSPLIT model at 3 altitudes (see Sect. 3.4) over each station for the overall period from 11–16 March 2008. Those aerosol scenarios are confirmed over the area under study with additional valuable information on the dust plume tracking. For simplicity, days representative of both no-dusty and dusty scenarios in each station have been selected: 11 March, 13 March and 14 March 2008. Plots of 5-day backtrajectories ending at SCO (square line), ARN site (triangle line) and GRA (circle line) sites for these selected days are shown in Fig. 4.

All air masses (independently on the altitude and site) arrive mostly from the ocean in no-dusty days. However, those arriving at 1500 m height over ARN and GRA stations had previously crossed the Iberian Peninsula for 6–9 h (see Fig. 4d,e), carrying a small aerosol (rural/continental) contribution (AOD < 0.1) as clearly observed by lidar measurements taken over both ARN and GRA sites at that altitude (see next sections).

Under dusty conditions on 12–13 March, all air masses arrive at SCO site from Saharan region. A day later (14 March), a change in wind direction in ARN and GRA stations is observed. In particular, the air mass at 3000 m height, representative of the FT, is especially investigated because this air mass is coming from the Mauritania and Western Sahara and most likely corresponds to the same Saharan air mass than that had crossed Tenerife just a day before (see Fig. 4h,i). Therefore, backtrajectory analysis confirms that the air masses observed over all three stations were originated in Saharan region, and that 3-km height air mass had travelled progressively through

over all three stations.

5.2 Vertical monitoring of dust plume: lidar measurements

5.2.1 Dust extinction layering structure

Vertical characterization of these Saharan dust plumes is focused on their height-resolved monitoring by using lidar measurements along the dust pathway over all three stations.

Height-resolved extinction is reported for each site (SCO, ARN and GRA) under no-dusty and dusty conditions. Only discrete dust extinction hourly-averaged (1-h) profiles are retrieved at discrete times because lidar data inversion is prevented by random cloud contamination for the overall observational period. Anthropogenic/marine aerosol contribution is also examined as a source of uncertainties introduced in that vertical dust characterization, if necessary. Next, particular aerosol profiling is examined in detail for each station.

a) SCO aerosol profiling

No-dusty conditions are found over SCO site before and after the 4-day Saharan dust intrusion (13–16 March 2008) as indicated by AERONET data and HYSPLIT backtrajectory analysis (see Sect. 5.1). Daily mean AOD^{500} values were quite low (AOD^{500}<0.15) with the $AE^{440/675}$ ranging from 0.7 to 1.2 in these no-dusty days of the overall monitored period. This atmospheric state represents typical clean marine conditions over coastal sites (i.e., Cattrall et al., 2005) like SCO station. In particular, the no-dusty case over SCO site on 11 March is examined. Aerosol profiling shows a layer confined in the marine boundary layer (MBL) at heights lower than 1.2 km. Vertical extinction coefficients at 12:00 UTC (1-h averaged profiles) over SCO site are shown in Fig. 5-left.

Regarding the fact that SCO station is a coastal site, marine contribution to aerosol profiling is steady. Therefore, a two-component aerosol system in a well differentiated

two-layer atmosphere is considered for lidar data retrieval (Ansmann, 2006) during that dust event over SCO station. In these dusty days, two aerosol dusty scenarios are proposed: 1) a "pure-dust" scenario (PDS), where dust particles are assumed as the principal aerosol component present in the overall atmosphere (no aerosol-type discrimination), and 2) a "mixed-dust" scenario (MDS), where a mixture of marine and dust particles are supposed to be present in the boundary layer (BL), and only dust in the free troposphere (FT). By this procedure, as reported by Cordoba-Jabonero et al. (2010), the marine aerosol contribution can be considered as a source of uncertainties introduced in that vertical dust characterization by data inversion processing.

Applying this procedure, in particular on 13 March, the day selected as representative for the 4-day dusty event over SCO site, a multilayered structure slightly varying along the day is found in each dusty scenario, with a higher dust contribution at BL heights for the PDS case, as expected by those inversion input conditions. Dust intrusion top is reached at around 4.5 km height, with the principal dust contribution, a 2.5 km width layer, extended from 1.5 to 4.0 km height. In this layer a dust enhanced peak is observed at around 3 km height during morning hours. Lidar-retrieved height-resolved dust extinction at selected averaged times for each dusty scenario is shown in Fig. 6.

As expected, when AERONET AOD constraint is applied for data retrieval (see Sect. 3.1.3), dust profiling is enhanced at FT altitudes (>1.2 km) as decreased at BL heights (<1.2 km) for the MDS case in comparison to the PDS one. In particular on 13 March, the daily mean dust contribution to the total AOD at FT heights over SCO was 69%±2% for the MDS case, higher by comparison with that 58%±3% as obtained for the PDS. These results highlight the importance of the aerosol scenario selected for lidar data retrieval (Cordoba-Jabonero et al., 2010). Accordingly, these results are also reflected in the retrieved LR data, as exposed in next section.

b) ARN and GRA aerosol profilings

A similar analysis of the lidar measurements is performed for both ARN and GRA sites.

Aerosol no-dusty conditions are found over both ARN and GRA sites just before and after the 1-day Saharan dust intrusion (14 March 2008) as indicated by AERONET data and HYSPLIT backtrajectory analysis (see Sect. 5.1). In particular, the case for 13 March is examined, and the vertical extinction coefficients in no-dusty conditions at noon (1-h averaged profiles) over ARN and GRA sites are shown in Fig. 5-centre and Fig. 5-right, respectively. In this case, aerosol vertical structure over ARN station is different to that obtained over SCO site: no significant presence of BL aerosols is observed. A small aerosol contribution is only found at around 1500 m. This result is in agreement with backtrajectory analysis presented before in this work (see Sect. 5.1.2): those air masses arriving at 1500 m (triangle line in Fig. 4e) had previously crossed the Peninsula for a few hours, likely carrying a small aerosol (anthropogenic/continental) contribution (AOD < 0.1, see Table 2) at these altitudes. Similar results are also found for GRA station (circle line in Fig. 4e), but in this case, such a contribution is smaller. Looking at the GRA profiles, it must be taken into account the higher altitude of this station (680 m a.s.l.).

Lidar retrieval of extinction coefficients is also performed for the 1-day dusty episode (14 March 2008) at a few discrete times due to cloud contamination. Lidar-retrieved height-resolved dust extinction at those discrete times (1-h averaged profiles) for both ARN and GRA sites is shown in Fig. 7-centre and Fig. 7-right, respectively (SCO profiling is also shown in this figure for comparison purposes). Examining the aerosol extinction, dust structure presents an extended layer ranging from 2.0 to 4.5 km height, being more remarkable for ARN site. In this situation, with no significant presence of BL aerosols, only one of the two previously proposed aerosol dusty scenarios is considered for data retrieval: the PDS case without any anthropogenic/marine contribution at BL altitudes. Dust particles are mostly confined in a single layer of 2.0–2.5 km width at FT altitudes, unlike SCO site where a multilayered dust structure extending from BL to FT levels was observed. Enhancement of aerosols in the mentioned layer one day after the air masses crossed Tenerife area confirms that the three stations were affected by the same Saharan air masses. That dust layer at 3 km height over the

Southern Iberian Peninsula as detected by lidar instrumentation at both ARN and GRA stations is directly related to that dust plume observed over Tenerife at 3 km height, as stated before by backtrajectory analysis (see Sect. 5.1, and in particular Fig. 4i). Moreover, GRA site also presents an aerosol contribution at heights lower than 2.0 km. This is likely due to local anthropogenic aerosol sources. This result is also reflected in the high AOD values registered in GRA site compared to those measured at rural ARN station (see Table 2).

5.2.2 Extinction-to-backscatter ratio (LR) retrievals

Lidar-retrieved LR (extinction-to-backscatter ratio) values, considering AERONET daily mean AOD as a constraint condition (see Sect. 3.1.3 for data processing details), are obtained for each aerosol scenario: LR=24 sr, 31 sr and 30 sr under no-dusty conditions, and LR=52 sr, 65 sr and 70 sr under PDS conditions, for SCO, ARN and GRA sites, respectively. In the MDS case, a LR value of 69 sr is retrieved for SCO station when a LR=35 sr is fixed at BL heights (<1.2 km). This former value is assumed as representative for the mixed state (mixture of marine and dust particles) of the SCO boundary layer for elastic lidar data inversion (AERONET AOD constrain) (Cordoba-Jabonero et al., 2010). These results are in good agreement with previously reported values based on lidar measurements of dust intrusions (i.e, Mona et al., 2006; Müller et al., 2003, 2007; Papayannis et al., 2008; Guerrero-Rascado et al., 2009).

Both AERONET-derived (see Table 2) and lidar-retrieved sets of LR values obtained for the overall monitored period at each station are shown in Fig. 8, where also the LR ranges adopted for different aerosol types are marked (dashed arrows): marine (20–30 sr), mixed (30–45 sr) and dust (45–70 sr). This LR criterion for aerosol-type discrimination is based on results from different previous works, including both lidar and AERONET retrievals. A summary of the LR values obtained by those reference works together with other information is shown in Table 3. CALIPSO (Cloud-Aerosol Lidar and Infrared Pathfinder Satellite Observation, http://www-calipso.larc.nasa.gov) LR-defined values are also shown for comparison.

Independently on the observational site, AERONET-derived LR values (open symbols, see legend in Fig. 8) are, in general, overestimated under no-dusty conditions, but underestimated in the presence of dust in comparison with the lidar-retrieved ones (solid symbols, see legend in Fig. 8). This AERONET LR underestimation under dusty conditions is also observed by other authors (i.e., Müller et al., 2007, 2010). LR values depend on chemical composition (refractive index), particle shape and size distribution. Therefore these differences found between both datasets for dust, non-spherical particles, may in part be caused by an insufficient understanding of the light-scattering model, highly shape-dependent, that is used in the AERONET data inversion algorithm (Müller et al., 2010). The AERONET LR overestimation under no-dusty conditions is also obtained by Landulfo et al. (2003) at São Paulo area, where no-dust (marine, continental, urban and biomass burning) aerosol case studies were only present. These results indicate the special features of dust particles in order to assess its impact into the radiative balance of the atmosphere, among other questions, in dependence on the methods/techniques used for dust characterization.

Important differences in LR values among these three stations are not found. This result can reflect that dust particles travelling in the same air mass plume have conserved their optical properties during that medium-range pathway. The small differences found in the dust properties measured in these stations can be associated to aging processes (chemical transformations along the tracking) and size distribution variations.

5.3 Potential impact on surface of the medium-range transported dust plume once over the Southern Iberian Peninsula

5.3.1 Surface air masses analysis

Lidar measurements showed that the dust plume is travelling between 2.5 and 4.5 km over the Iberian Peninsula, as observed at ARN and GRA stations on 14 March, after crossing a day before the Canary Islands, and in particular SCO station. HYSPLIT backtrajectories clearly show a Saharan origin of these dust air masses (see Fig. 4).

They were following an Atlantic arch through the Canary Islands as favoured by meteorological situation in that area before reaching the Southern Iberian Peninsula. In order to get a better picture on what is going on below that Saharan dust plume at rather lower heights, a brief analysis of the origin of the air masses arriving at closest-to-surface altitudes over ARN and GRA stations is performed.

HYSPLIT 5-day backtrajectories ending at both ARN and GRA sites at 500 m a.g.l. indicate that air masses come directly from the Northern and Northwestern African continent, influencing ARN station on 14 March from 06:00–14:00 UTC and from 14 March at 15:00 UTC to 15 March at 09:00 UTC, respectively. In the case of GRA site, they also arrive from Northern Africa from 14 March at 14:00 UTC to 15 March at 10:00 UTC but after crossing previously the Iberian Peninsula. After 15 March at 06:00 UTC air masses do not come from desert areas. Those air mass backtrajectories ending at 500 m a.g.l., representative of the surface impact at ground level of the dust episode, are shown in Fig. 9 over both ARN (triangle line) and GRA (square line) sites.

In addition, air masses ending at ARN site have been crossing the desert area for a longer time and have arrived from a higher height (about 1500 m a.g.l.) than those ending at GRA site (see Fig. 9a,b). According to backtrajectories, these air masses seem not to be related with the upper 3-km height dust plume. However, surface in situ measurements must be examined to confirm this preliminary result and the potential dust impact on surface.

5.3.2 Surface in situ observations: ground-level measurements

Both size-resolved and optical properties at ground level are investigated with the aim to evaluate the impact of desert dust aerosol over ARN and GRA sites. Unfortunately, due to the limitations of the sun-photometric observations (only daytime data can be obtained and under clear sky conditions), microphysical derived columnar-integrated data, including size-resolved distributions, coincident with the duration of the dust event are not available. Therefore, no comparison with in situ measurements can be performed.

a) Size-resolved measurements

Particle volume size distribution has been used in this work since this magnitude, better than number or surface, represents the ground-level sediment mass. Although the particle number is small, coarse mode is a significant or even dominant contribution to the total loading. Temporal evolution of the total volume particle concentration (TV) is presented for four discrete size ranges: 0.01–0.4 µm (TV0), 0.5–1.0 µm (TV1), 1.0–2.5 µm (TV2) and 2.5–10.0 µm (TV3) for the overall period of 12–16 March 2008 in both ARN (see Fig. 10a,b) and GRA (see Fig. 10c,d) sites (no TV0 data are available in GRA station). Three different kinds of aerosol episodes are selected to illustrate the aerosol particle size-resolved features: 1) the Regional Anthropogenic Plume (RAP) episode, presenting an increase of volume concentration predominantly for sub-micrometer particles (TV0 and TV1); 2) the Desert Dust Plume (DDP) episode, with a predominance of micrometer-size (>1 µm, i.e., TV2 and TV3 ranges) particles over the total volume concentration; and 3) the Diurnal Pattern (DP) scenario, characterized by local environmental conditions controlling the particle sources of sub- (TV1) and micrometer- (TV2 and TV3) sizes. These selected aerosol episodes are marked by grey arrows (RAP and DP) and dashed areas (DDP) in Fig. 10.

RAP episodes appear in ARN site (Fig. 10a,b) when wind was blowing from Northern direction, where a cement factory is located at about 30 km far from this station. The strongest RAP episode is observed from the second half of the day 13 March to the next early morning. During this episode, both TV0 and TV1 concentrations increase by 2.8 and 3.5, respectively. At the same time, TV2 concentration shows the same behaviour but at a smaller scale.

During DP episodes in GRA station, the volume concentration presents a clear diurnal pattern with two local maxima around 08:00 UTC and 19:00 UTC during working days (see Fig. 10c,d), caused by local traffic and atmospheric boundary layer activities, as also indicated in previous published works (Lyamani et al., 2008, 2010). The early morning maximums of TV1, TV2 and TV3 concentrations are 1.7±0.5, 1.5±0.2 and

1.3±0.3 times on average higher, respectively, than their evening maximums. Morning DP event on 12 March is selected as representative of local traffic impact over volume size distributions in GRA site. TV1, TV2 and TV3 concentrations increase by 4.0, 4.6 and 7.0 times, respectively.

Therefore, DP episodes at GRA station and LP events at ARN site produce a similar impact on the concentration of submicrometer-size particles (TV1). However, DP episodes at GRA generate a higher effect on the concentration of micrometer-size particles than LP events at ARN. By comparison between both stations, TV1 concentrations are similar in both rural-coastal (ARN) and urban (GRA) environments. This result can be associated to marine aerosol presence over ARN site, and local anthropogenic particles in GRA station. Regarding TV2 and TV3 particles, their concentrations are higher in GRA site, with peak values at working days mainly related to re-suspended aerosols by road traffic.

The analysis of the DDP episode allows assessing the impact on surface and the duration of the Saharan dust intrusion plume examined in this work. A difference of 8 h on dust event detection is observed between both stations, as also observed by HYSPLIT backtrajectory analysis at ground level (see Sect. 5.3.1 and Fig. 9). That dust plume travelling coincides with the temporal evolution presented in Fig. 10, and therefore surface in situ measurements confirm the DDP episode over both ARN and GRA stations at ground-level surface.

The highest impact of DDP episode over ARN station (see Fig. 10a,b) is observed on the TV3 concentration, from 14 March at 06:00 UTC to 15 March at 03:00 UTC. Persistent TV3 levels of about 10 $\mu m^3\,cm^{-3}$ are observed on 14 March at 14:00 UTC, when the air masses affecting ARN station are crossing at higher altitudes over Northwestern African continent (see Sect. 5.3.1). The highest TV1 and TV2 concentrations in ARN site were registered on 15 March at 00:00 UTC, 10 h later than TV3 maximum levels. During this episode, the TV1 and TV2 concentrations increase by a factor of 2. The highest TV0 concentration in ARN is registered on 15 March at 3:00 UTC, 3 h later than TV3 highest levels, increasing by more than 2 times for this event. These fine particles belong to the DDP episode, since their enhancement and evolution coincide with that of TV3 particles and the wind was blowing from the Southwest (ocean direction) but not from the Northern direction, where the cement factory is placed. In the case of GRA DDP episode (see Fig. 10c,d), the TV3 concentration reaches its maximum 9 h later than the TV1 and TV2 concentrations are in their highest levels. A simplified chronology with the most relevant features of the DDP episode for each particle size range is shown in Table 4 for both ARN and GRA sites.

Comparing these results obtained in both stations, the highest impact of this DDP event on background concentration levels is observed in GRA site. These results agree with the backtrajectory analysis (see Sect. 5.3.1) showing that the air masses arriving at GRA station during this episode come from rather lower heights, even touching the surface, than those reaching ARN site (from 1500 m height). This result is also supported by lidar measurements showing no dust incidence from around 1800 m height down to surface (see Fig. 7).

Regarding the temporal evolution of the DDP TV particle concentrations during the DDP episode (see Table 4), differences are observed between both sites in relation with the deposition process. In ARN large particles are deposited on surface before the small ones, and TV2 concentration increase is detected at ground level with a 10-h delay respect to the TV3 concentration. However, the maximum TV3 concentration in GRA station is detected with a 9-h delay respect to TV2. This opposite result can be related to the gravitational deposition process in ARN from the 3-km height dust layer as observed by lidar measurements (see Sect. 5.2) whereas in GRA, particles at ground level are coming directly from the Africa continent. First deposition behaviour corresponds to the fact that larger particles (>2.5 µm) settle down faster than smaller ones (<2.5 µm) by gravitational process, being then first detected in ARN site, while the second ones are associated to a slower horizontal velocity of sedimentation for large particles (TV3), arriving later at GRA station.

Selected particle volume size distributions (VSD) (hourly averaged) at ground level under dusty and no-dusty conditions are presented in Fig. 11a,b for ARN and GRA

sites, respectively. The VSD in ARN site have been smoothed due to the high coarse mode data variability introduced by large statistical errors. As the event proceeds deposition is shifting from coarse mode to fine mode. A representative VSD for the beginning of dust event can be observed on 14 March at 09:00 UTC in ARN site. Sedimentation of large particles takes place on 14 March at 15:00 UTC (see Fig. 11a), with a coarse modal diameter estimation of about 7 µm. Few hours later, on 15 March at 02:00 UTC, the contribution of small (<2.5 µm) particles increases, with fine and coarse modal diameters of 0.2 µm and 2.2 µm, respectively. Finally, on 15 March at 05:00 UTC, VSD is characterized by the deposition of submicrometer particles, being the fine and coarse modal diameters of 0.35 µm and 2.0 µm, respectively.

These four selected dusty distributions present a ratio of the fine mode to total mode VSD ($V_{F/T}$) of 0.54, 0.29, 0.26 and 0.60, respectively. Finally, VSD on 15 March at 12:00 UTC is representative of no-dusty conditions with modal diameters of 0.2 µm and 2.3 µm for the fine and coarse modes, respectively, and a $V_{F/T}$ of 0.34. $V_{F/T}$ values of around 0.1 correspond to the presence of desert dust particles as based on previous results on columnar-integrated aerosol characterization in ARN site (Prats et al., 2008), where regular values below 0.5 were reported. According to the results obtained during the desert dust event analyzed in this work, the highest dust impact over ARN site occurs on 14 March at 15:00 UTC and 15 March 02:00 UTC when lower $V_{F/T}$ are found, i.e. around 0.28, a value higher than that 0.1 reported by Prats et al. (2008). This result highlights the underestimation provided by the columnar-integrated data to the fine mode particle contribution under dusty conditions in comparison with that obtained by surface in situ measurements.

VSD evolution over GRA site is shown in Fig. 11b, which is only evaluated by using APS system measurements (no instrumentation for particles <0.4 µm size detection is in GRA). Typical no-dusty VSD are found before 14 March at 00:00 UTC and after 15 March at 19:00 UTC. During the first phase of the dusty episode, VSD presented an increase of micrometer-size particles, mainly within the TV2 particle range, as shown on 14 March at 19:00 UTC and 15 March at 02:00 UTC in Fig. 11b. For these cases,

a modal diameter of 1.8 µm is obtained. Impact of large particles is represented for the VSD on 15 March at 07:00 UTC, with a modal diameter of 5.1 µm. In the course of the dust event, coarse mode particles increased. The sequence is the opposite of that found in ARN site only 250 km away.

Unfortunately, as stated before, comparison between both columnar-integrated and ground-level datasets has not been possible since AERONET-derived microphysical data (level 2 inversions) are not available during the dusty episode over both ARN and GRA stations.

b) Aerosol optical properties

Scattering coefficient at 550 nm (SC^{550}), Angstrom exponent (550/700 nm wavelength pair, $AE_{np}^{550/700}$) and backscatter fraction at 550 nm (BSC^{550}) for surface particles with a diameter lower than 10 µm are also examined, as representatives of optical properties, along the overall monitored period. Temporal evolution of these parameters SC^{550}, $AE_{np}^{550/700}$ and BSC^{550} (hourly averaged values) in both ARN and GRA stations is shown in Fig. 12a,b, respectively. During RAP episode at ARN station (see Fig. 12a), the SC^{550} presents a large enhancement, increasing from 30 Mm^{-1} to 123 Mm^{-1}, and its maximum value coincides with the peak observed in TV0 and TV1. A mean $AE_{np}^{550/700}$ value of 1.8±0.1 is obtained for this event, indicating a predominance of fine particles. As representative of GRA DP event (see Fig. 12b), the episode occurred on 13 March is selected. SC^{550} values obtained during this event are similar to those obtained for the RAP episode at ARN station. A mean $AE_{np}^{550/700}$ value of 1.5±0.3 is obtained, indicating a predominance of fine particles. Both episodes (RAP and DP) with different origin present similar scattering properties, with differences in the particle micrometer-size range (see previous analysis of this section).

During the ARN DDP episode hourly-averaged $AE_{np}^{550/700}$ values decreased from 1.88 to 0.45. Mean $AE_{np}^{550/700}$ and SC^{550} values of 1.1±0.4 and 43±18 Mm^{-1}, respectively, were obtained. The highest impact of this DDP episode in ARN site shows an

increase of the TV3 concentration with the lowest $AE_{np}^{550/700}$ and BSC^{550} values, indicating a dominance of those large aerosols over the scattering process (see Fig. 9, Fig. 10a,b). A mean $AE_{np}^{550/700}$ value of 0.7±0.2 is found for this intense period, in agreement with previous reported results on dust optical properties (i.e., Kim et al., 2005), and also similar SC^{550} values for the overall DDP period to those analyzed in White et al. (1994) and Chang et al. (2006). In the case of GRA station, the DDP $AE_{np}^{550/700}$ decreased from 0.89 to 0.32, with a mean value of 0.7±0.3. A mean SC^{550} value of 71±25 Mm^{-1} was found for this dusty period. These results for $AE_{np}^{550/700}$ and SC^{550} are similar to those obtained by Kalivitis et al. (2007) and Pereira et al. (2008).

By comparing the results obtained in both Southern Iberian Peninsula stations, SC^{550} values are around 1.6 times higher in GRA than those obtained in ARN station during the DDP episode, because of the significant contribution from local anthropogenic sources in the urban GRA site. In addition, lower $AE_{np}^{550/700}$ values found in GRA station are in agreement with the high TV2 and TV3 concentrations observed in GRA site (see Fig. 10). SC^{550} values for both stations during the DDP episode are lower than those found for typical sites with higher local pollution levels, which contribute to high aerosol loadings during the DDP event (Kim et al., 2005; Chang et al., 2006).

In order to evaluate the aerosol effectiveness on solar light radiation, the mass scattering coefficient efficiency at 550 nm (SC_m^{550}), defined as the ratio of SC^{550} to the aerosol total mass concentration (TM) (i.e., Kalavitis et al., 2007) is determined. In this work, TM is calculated by the product of the effective density (2 g cm^{-3} is assumed) and the volume size distribution (VSD). Since SC^{550} is obtained for particles with sizes lower than 10 µm and no TV0 concentration is available in GRA station, the analysis is performed only for ARN station. Lineal regression of SC^{550} versus TM is shown in Fig. 13 for the RAP event (open circles) and the DDP episode (full squares). In both cases high correlation coefficients (C.C.) of 0.86–0.87 are obtained, indicating a good relation between optical and microphysical parameters. SC_m^{550} values of

0.88±0.04 $m^2\,g^{-1}$ and 2.3±0.2 $m^2\,g^{-1}$ are found for dusty and no-dusty periods, respectively. Therefore, anthropogenic industrial particles are 2.5 times more efficient for solar light scattering than dust particles. These values are in good agreement with others previously reported for the same kind of aerosols (Kim et al., 2005; Chang et al., 2006; Pereira et al., 2008).

5.3.3 Dust particle sedimentation

From previously exposed backtrajectory and size-resolved analysis, it came out that the origin of the DDP episode observed at ground level in both ARN and GRA stations is from the Northern Africa. But those air masses arrive at closest-to-surface heights over both stations instead of coming from that observed 3-km height dust plume with a Saharan-Tenerife pathway, as shown by lidar measurements and HYSPLIT backtrajectories (see previous sections). These results can be justified in relation with the suspension time estimated for these dust particles till their deposition on the surface.

Examining the 3-km wind fields provided by the BSC/DREAM (Barcelona Supercomputing Center/Dust REgional Atmospheric Model, http://www.bsc.es/projects/earthscience/DREAM/) dust model (data not shown), the dust plume at these altitudes was traveling with a speed of about 40 km h^{-1}, and it took 30 h to reach the southern coast of the Iberian Peninsula. On the other hand, particle sedimentation depends on size, density and air viscosity (Hinds, 1999; Osborne and Haywood, 2005). For small particles with sizes approaching to the mean free-path of the gas, there is a "slip" of the particle (the relative velocity of the gas at the surface of the particle is cero) and the pressure-dependent Cunningham correction factor has to be included in the Stoke's equation. The differences start to be meaningful above 1 µm in diameter (Hinds, 1999; Osborne and Haywood, 2005). Saharan dust 10- µm size particles traveling at 3000 m sediment by 600 m d^{-1}, while 5- µm particle settling is only of 200 m d^{-1}.

In consequence, rather low particle sedimentation is expected to occur before the dust plume reaches the south coast of Iberian Peninsula. This confirms the surface in

situ results obtained for both ARN and GRA stations, as stated before.

6 Conclusions

The relevance of the synergetic use of simultaneous remote sensing and in situ observations for aerosol research is highlighted in this work. Meteorological information, AERONET data, lidar observations, backtrajectory analysis and surface in situ measurements have been used for characterization of dust intrusions coming from Saharan region. A medium-range dust plume transported from the Canary Islands to the Iberian Peninsula, relatively located close and far away from the dust sources, respectively, have been exhaustively monitored from 11–19 March 2008. Observations were performed over three Spanish geographically strategic within the dust-influenced area stations along a common dust plume pathway: Santa Cruz de Tenerife Observatory (SCO, AEMET) in the Canary Islands, and the Atmospheric Sounding Station "El Arenosillo" (ARN, INTA) and the Granada Station (GRA, UGR) in the Southwest and Southeast of the Iberian Peninsula, respectively. A 4-day dust event was detected over SCO station lasting from 13–16 March 2008; the same dust air mass was observed over the South of the Iberian Peninsula on 14 March 2008 at both ARN and GRA sites.

Meteorological situation over the area under study favoured the dust plume transport from Saharan region to Canary Islands, and then to the Southern Iberian Peninsula. Backtrajectory analysis shows a common Saharan origin of the dust air masses over all the stations at 3-km height. AERONET data have been used to confirm the dust particles loading in those plumes in basis of selected AOD and AE ranges: daily mean moderate/high AOD values (0.3–0.6) together with low AE<0.5 are found over all three stations for each dust intrusion.

Lidar observations have characterized the vertical layering structure of those dust plumes, identifying different aerosol contributions depending on altitude. Dust layer tops are found at 4.5–5.0 km height in all stations. SCO extinction profiling displays a multilayered structure through the overall atmosphere up to the top meanwhile ARN

and GRA profiles present mainly a single dust layer of 2.0 km thick confined between 2.5 and 4.5 km height and peaking at about 3.2 km. Backtrajectories at these height levels confirm the Saharan origin of the plume moving through Canary Islands and observed over SCO site, before reaching the Iberian Peninsula. In addition, a minor aerosol (continental/anthropogenic) contribution is observed in GRA station below 2.5 km related to air masses crossing through the Iberian Peninsula before reaching that station, as also confirmed by backtrajectory analysis. Lidar-retrieved LR values have been estimated for each station, being decisive the selection of the aerosol scenario for data retrieval. Realistic aerosol conditions over SCO station are obtained when using the proposed "mixed dust" scenario (MDS) with aerosol-type discrimination. LR values of 24 sr, 31 sr, and 31 sr are found under no-dusty conditions, and 69 sr, 65 sr and 70 sr for the principal dusty episodes over SCO, ARN and GRA sites, respectively. The similar values obtained in all three stations provide evidence on that the dust plume properties keep unchanged in the course of its medium-range transport. These values are in good agreement with those previously reported for dust particles (i.e., Müller et al., 2007; Papayannis et al., 2008). However, LR for dust particles are underestimated if AERONET retrieved data are used.

Moreover, the potential impact on surface of that Saharan dust plume arriving at the Iberian Peninsula has been evaluated by ground-level in situ measurements for particle deposition assessment. An 8 h delay on dust arrival times at ground level between ARN and GRA sites is found. Differences on particle deposition process are observed in both sites by using the temporal evolution of the TV particle concentration for discrete size ranges. Meanwhile TV3 (2.5–10 µm) size particles are detected 10 h before than TV2 (1.0–2.5 µm) ones in ARN, the particle behaviour over in GRA is just opposite. The TV2 particles arrived 9 h before than the larger TV3 one. These differences can be explained by the particular transport pattern occurred in each station. Backtrajectory analysis confirms those closest-to-surface air masses arriving at both sites from the North Africa continent, coming to GRA site from lower heights than those reaching ARN station. Therefore, particles over ARN station would be the result of a gravita-

tional deposition process, while those in GRA station would be mostly influenced by their horizontal movement. The first behaviour is related to the faster gravitational deposition (vertical velocity) for larger particles than smaller ones, and the second one is associated to a slower horizontal movement for the large particles.

A more detailed analysis of the backtrajectories ending at several heights over each station reveals that those closest-to-surface air masses are coming directly from Northern African continent, whereas those ending at 3-km carrying the dust plume are coming from the considered Sahara-Tenerife-Iberian Peninsula pathway. That is also confirmed by sedimentation analysis based on particle size, density and air viscosity computation. The deposition process starts to be meaningful for particles above 1 µm in diameter, but even for dust 10- µm size particles, the sedimentation would be by 600 m d^{-1}, i.e., dust plume particles travelling at 3-km height take 5 days to reach the surface. In consequence, rather low particle sedimentation is expected to occur directly from the dust 3-km height plume once reached the Southern Iberian Peninsula. Therefore, dust particles registered at ground level are not related to deposition processes for particles of that monitored dust plume, being thus its potential impact on surface rather low. However, dust incidence really exists in relation with those surface air masses arriving from the Northern Africa continent, as stated before. The dust event as monitored on the ground level over Southern Iberian Peninsula presents a higher incidence in the Southeastern region respect to the Southwestern area by comparison of both TV2 and TV3 concentrations registered over both GRA and ARN stations. In addition, both optical parameters SC^{550} and $AE_{np}^{550/700}$ obtained in GRA site are 1.6 higher and 1.7 lower, respectively, than those found in a rural/coastal environment like ARN station. Furthermore, aerosol effectiveness on solar light interaction is evaluated in ARN station on the basis of the mass scattering coefficient SC_m^{550}, resulting in a value close to 0.9 m^2 g^{-1} for dust and 2.3 m^2 g^{-1} for regional anthropogenic industrial aerosols. This indicates the former particles are 2.5 times more efficient for solar light scattering than dust particles.

In summary, synergetic, i.e. multi-instrumented and simultaneous, use of: 1) meteorological information; 2) height-resolved dust structure obtained by lidar measurements; 3) optical/microphysical properties derived from AERONET columnar-integrated data; and 4) both horizontal and vertical backtrajectory analysis of air masses, in different aerosol stations, represents an important advantage for the characterization of dust properties in the course of their transport from desert source regions as far as their surface deposition. Moreover, ground-level in situ measurements together with closest-to-surface backtrajectory analysis provide a relevant tool to discriminate different deposition processes and highlight the aerosol-dependent relation between microphysical and optical properties.

In particular, this work can be presented as a first step to organize a Spanish Warning System for Saharan dust intrusions that frequently affect the Canary Islands and the Iberian Peninsula based on both ground-based active (lidar) and passive (sunphotometry) remote sensing, backtrajectory analysis and surface in situ measurements. Obtained results can be used as a reference for dust monitoring over other dust-influenced regions.

Acknowledgements. This work has been supported by the Spanish Ministry for Science and Innovation (MICINN) under the Acciones Complementarias CGL2006-26149-E/CLI (2007), CGL2007-28871-E/CLI (2008) and CGL2008-01330-E/CLI (2009) in the frame of the Spanish and Portuguese Aerosol LIdar NETwork (SPALINET); projects CGL2008-05939-C03-03/CLI, CGL2007-66477-C02-01, CSD2007-00067 and CGL2004-05984-C07-03 of the Spanish Ministry of Education; projects P08-RNM-3568 and P06-RNM-01503 of the Autonomous Government of Andalusia; and the EARLINET-ASOS project (EU Coordination Action, contract n° 025991 (RICA)). Authors would like to express their gratitude to the NOAA Air Resources Laboratory (ARL) for the HYSPLIT backtrajectories, the NOAA/ESRL Physical Sciences Division in Boulder Colorado for the meteorological synoptic charts, the Barcelona Supercomputing Centre (BSC) for the DREAM forecast and EUSAAR Project for providing technical support for in situ equipment in ARN. JLG-R thanks the Fundação para a Ciência e a Tecnologia for supporting under grant SFRH/BPD/63090/2009.

References

Alados-Arboledas, L., Lyamani, H., and Olmo, F. J.: Aerosol size properties at Armilla, Granada (Spain), Q. J. Roy. Meteor. Soc., 129, 1395–1413, 2003.

Alados-Arboledas, L., Alcantara, A., Olmo, F. J., Martinez-Lozano, J. A., Estelles, V., Cachorro, V., Silva, A. M., Horvath, H., Gangl, M., Diaz, A., Pujadas, M., Lorente, J., Labajo, A., Sorribas, M., and Pavese, G.: Aerosol columnar properties retrieved from CIMEL radiometers during VELETA 2002, Atmos. Environ., 42, 2654–2667, 2008.

Anderson, T. L. and Ogren, J. A.: Optimal determination of aerosol radiative properties using the TSI 3563 nephelometer, Aerosol Sci. Tech., 29, 57–69, 1998.

Andreade, M. O.: Climatic effects of changing atmospheric aerosol levels, in: World Survey of Climatology, 16, Future Climates of the World, edited by: Henserson-Sellers, A., Elsevier, Amsterdam, 341–392, 1995.

Angstrom, A.: The parameters of atmospheric turbidity, Tellus, 16, 64–75, 1964.

Ansmann, A.: Ground-truth aerosol lidar observations: can the Klett solutions obtained from ground and space be equal for the same aerosol case?, Appl. Optics, 45(14), 3367–3371, 2006.

Ansmann, A., Bösenberg, J., Chaikovsky, A., Comeron, A., Eckhardt, S., Eixmann, R., Freudenthaler, V., Ginoux, P., Komguem, L., Linne, H., Lopez Marquez, M. A., Matthias, V., Mattis, I., Mitev, V., Müller, D., Music, S., Nickovic, S., Pelon, J., Sauvage, L., Sobolewsky, P., Srivastava, M. K., Stohl, A., Torres, O., Vaughan, G., Wandinger, U., and Wiegner, M.: Long-range transport of Saharan dust to Northern Europe: the 11–16 October 2001 outbreak observed with EARLINET, J. Geophys. Res., 108(D24), 4783, doi:10.1029/2003JD003757, 2003.

Balis, D., Papayannis, A., Galani, E., Marenco, F., Santacesaria, V., Hamonou, E., Chazette, P., Ziomas, I., and Zerefos, C.: Tropospheric LIDAR aerosol measurements and sun photometric observations at Thessaloniki, Greece, Atmos. Environ., 34(6), 925–932, 2000.

Balis, D. S., Zerefos, C. S., Kourtidis, K., Bais, A. F., Hofzumahaus, A., Kraus, A., Schmitt, R., Blumthaler, M., and Gobbi, G. P.: Measurements and modeling of the photolysis rates during the photochemical activity and ultraviolet radiation (PAUR) II campaign, J. Geophys. Res., 107(D18), 8138, doi:10.1029/2000JD000136, 2002.

Balis, D., Amiridis, V., Nickovic, S., Papayannis, A., and Zerefos, C.: Optical properties of Saharan dust layers as detected by a Raman lidar at Thessaloniki, Greece, Geophys. Res. Lett., 31, L13104, doi:10.1029/2004GL019881, 2004.

Basart, S., Pérez, C., Cuevas, E., Baldasano, J. M., and Gobbi, G. P.: Aerosol characterization in Northern Africa, Northeastern Atlantic, Mediterranean Basin and Middle East from direct-sun AERONET observations, Atmos. Chem. Phys., 9, 8265–8282, doi:10.5194/acp-9-8265-2009, 2009.

Bonasoni, P., Cristofanelli, P., Calzolari, F., Bonafè, U., Evangelisti, F., Stohl, A., Zauli Sajani, S., van Dingenen, R., Colombo, T., and Balkanski, Y.: Aerosol-ozone correlations during dust transport episodes, Atmos. Chem. Phys., 4, 1201–1215, doi:10.5194/acp-4-1201-2004, 2004.

Cachorro, V. E., Toledano, C., Prats, N., Sorribas, M., Mogo, S., Berjon, A., Torres, B., Rodrigo, R., De la Rosa, J., and De Frutos, A. M.: The stronger desert dust intrusions mixed with smoke over the Iberian Peninsula registered with Sun photometry, J. Geophys. Res., 113, D14S04, doi:10.1029/2007JD009582, 2008.

Campbell, J. R., Hlavka, D. L., Welton, E. J., Flynn, C. J., Turner, D. D., Spinhirne, J. D., Stanley Scott III, V., and Hwang, I. H.: Full-time, eye-safe cloud and aerosol Lidar observation at atmospheric radiation measurement program sites: instruments and data processing, J. Atmos. Ocean. Tech., 19, 431–442, 2002.

Cattrall, C., Reagan, J., Thome, K., and Dubovik, O.: Variability of aerosol and spectral lidar and backscatter and extinction ratios of key aerosol types derived from selected aerosol robotic network locations, J. Geophys. Res., 110, D10S11, doi:10.1029/2004JD005124, 2005.

Chang, S.-Y., Fang, G-C., Chou, C. C.-K., and Chen, W.-N.: Chemical compositions and radiative properties of dust and anthropogenic air masses study in Taipei Basin, Taiwan, during spring of 2004, Atmos. Environ., 40, 7796–7809, 2006.

Cordoba-Jabonero, C., Gil, M., Yela, M., Maturilli, M., and Neuber, R.: Polar stratospheric cloud observations in the 2006/07 Arctic winter by using an improved micro pulse lidar, J. Atmos. Ocean. Tech., 26, 2136–2148, 2009.

Cordoba-Jabonero, C., Hernández, Y., Gil, M., and Cuevas, E.: Aerosol scenario effect in elastic lidar data inversion for lidar ratio estimation: a case study over a coastal dust-influenced area, Proceedings of the IV Reunion Española de Ciencia y Tecnologia de Aerosoles (RECTA 2010), Granada (Spain), 28–30 June, edited by: Alados-Arboledas, L., Olmo Reyes, F. J. Guerrero-Rascado, J. L., and Anton Martinez, M., Universidad de Granada, Granada, Spain, 2010.

Draxler, R. R. and Hess, G. D.: An overview of the HYSPLIT 4 modeling system for trajectories, dispersion, and deposition, Aust. Meteorol. Mag., 47, 295–308, 1998.

Draxler, R. R., Stunder, B., Rolph, G., and Taylor, A.: Hysplit 4 User's Guide, NOAA Air Resources Laboratory, Silver Spring, MD, 2009.

Dubovik, O. and King, M. D.: A flexible inversion algorithm for retrieval of aerosol optical properties from sun and sky radiance measurements, J. Geophys. Res., 105, 20673–20696, 2000.

Dubovik, O., Sinyuk, A., Lapyonok, T., Holben, B. N., Mishchenko, M., Yang, P., Eck, T. F., Volten, H., Muñoz, O., Veihelmann, B., van der Zande, W. J., Leon, J.-F., Sorokin, M., and Slutsker, I.: The application of spheroid models to account for aerosol particle nonsphericity in remote sensing of desert dust, J. Geophys. Res., 111, D11208, doi: 10.1029/2005GL06619, 2006.

Dulac, F., Attie, J-L., Bergametti, G., Mallet, M., Sciare, J., Tanre, D., Borbon, A., Coppola, L., Chazette, P., Desboeufs, K., Durand, P., Flamant, C., Gheusi, F., Gomes, L., Guieu, C., Lambert, D., Liousse, C., Losno, R., Marchand, N., Mari, C., Notton, G., Peuch, V.-H., Ravetta, F., Ricaud, P., Savelli, J.-L., Seigneur, C., Turquety, S., and Verdier, N.: The Chemistry-Aerosol Mediterranean Experiment (ChArMEx), 1st International Workshop, Toulouse (France), 29 June–1 July, Meteó France, Toulouse, France, 2009.

Escudero, M., Querol, X., Pey, J., Alastuey, A., Perez, N., Ferreira, F., Alonso, S., Rodriguez, S., and Cuevas, E.: A methodology for the quantification of the net African dust load in air quality monitoring Networks, Atmos. Environ., 41(26), 5516–5524, 2007.

Fernald, F. G., Herman, B. M., and Reagan, J. A.: Determination of aerosol height distribution by lidar, J. Appl. Meteorol., 11, 482–489, 1972.

Fernald, F. G.: Analysis of atmospheric lidar observations: some comments, Appl. Optics, 23, 652–653, 1984.

Gonzalez-Castanedo, Y., De la Rosa, J. D., Sanchez de la Campa, A., Alastuey, A., Querol, X., Cachorro, V., Sorribas, M., and Bolivar, J. P.: Levels, chemicals composition and mass contribution of particulate matter in a rural monitoring station, Proceedings of the 6^{a} Asamblea Hispano-Portuguesa de Geodesia y Geofísica, Tomar, Portugal, 11–14 February, 2008.

Guerrero-Rascado, J. L., Ruiz, B., and Alados-Arboledas, L.: Multi-spectral lidar characterization of the vertical structure of Saharan dust aerosol over Southern Spain, Atmos. Environ., 42, 2668–2681, 2008.

Guerrero-Rascado, J. L., Olmo, F. J., Avilés-Rodríguez, I., Navas-Guzmán, F., Pérez-Ramírez, D., Lyamani, H., and Alados Arboledas, L.: Extreme Saharan dust event over the southern Iberian Peninsula in september 2007: active and passive remote sensing from surface and satellite, Atmos. Chem. Phys., 9, 8453–8469, doi:10.5194/acp-9-8453-2009, 2009.

Hamonou, E., Chazette, P., Balis, D., and Papayannis, A.: Characterization of the vertical structure of Saharan dust export to the Mediterranean Basin, J. Geophys. Res., 104(D18), 22257–22270, 1999.

Holm, R. L., Caldow, R., Hairston, P. P., Quant, F. R., and Sem, G. J.: An enhanced time-of-flight spectrometer that measures aerodynamic size plus light-scattering intensity, J. Aerosol Sci., 28S1, S11–S12, 1997.

IPCC 2007: Climate Change and Water. Technical Paper of the Intergovernmental Panel on Climate Change, edited by: Bates, B. C., Kundzewicz, Z. W., Wu, S., and Palutikof, J. P., IPCC Secretariat, Geneva, 210 pp., 2008.

Kalivitis, N., Gerasopoulos, E., Vrekoussis, M., Kouvarakis, G., Kubilay, N., Hatzianastassiou, N., Vardavas, I., and Mihalopoulos, N.: Dust transport over the Eastern Mediterranean derived from Total Ozone Mapping Spectrometer, Aerosol Robotic Network, and surface measurements, J. Geophys. Res., 112, D03202, doi:10.1029/2006JD007510, 2007.

Kalnay, E., Kanamitsu, M., Kistler, R., Collins, W., Deaven, D., Gandin, L., Iredell, M., Saha, S., White, G., Woollen, J., Zhu, Y., Leetmaa, A., Reynolds, R., Chelliah, M., Ebisuzaki, W., Higgins, W., Janowiak, J., Mo, K.C., Ropelewski, C., Wang, J., Jenne, R., and Joseph, D.: The NCEP/NCAR reanalysis 40-year project, Bull. Amer. Meteor. Soc., 77, 437–471, 1996.

Kim, S.-W., Yoon, S.-C, Jefferson, A., Ogren, J. A., Dutton, E. G., Won, J.-G., Ghim, Y. S., Lee, B.-I., and Han, J.-S.: Aerosol optical, chemical and physical properties at Gosan, Korea during Asian dust and pollution episodes in 2001, Atmos. Environ., 39, 39–50, 2005.

Klett, J. D.: Stable analytic inversion solution for processing lidar returns, Appl. Optics, 20, 211–220, 1981.

Klett, J. D.: Lidar inversion with variable backscatter/extinction ratios, Appl. Optics, 24, 1638–1643, 1985.

Knutson, E. O. and Whitby, K. T.: Aerosol classification by electric mobility: apparatus, theory and applicantions, J. Aerosol Sci., 6, 443–451, 1975.

Landulfo, E., Papayannis, A., Artaxo, P., Castanho, A. D. A., de Freitas, A. Z., Souza, R. F., Vieira Junior, N. D., Jorge, M. P. M. P., Sánchez-Ccoyllo, O. R., and Moreira, D. S.: Synergetic measurements of aerosols over São Paulo, Brazil using LIDAR, sunphotometer and satellite data during the dry season, Atmos. Chem. Phys., 3, 1523–1539, doi:10.5194/acp-3-1523-2003, 2003.

Lyamani, H., Olmo, F. J., and Alados-Arboledas, L.: Long-term changes in aerosol radiative properties at Armilla (Spain), Atmos. Environ., 38, 5935–5943, 2004.

Lyamani, H., Olmo, F. J., and Alados-Arboledas, L.: Saharan dust outbreak over Southeastern Spain as detected by sun photometer, Atmos. Environ., 39, 7276–7284, 2005.
Lyamani, H., Olmo, F. J., Alcantara, A., and Alados-Arboledas, L.: Atmospheric aerosols during the 2003 heat wave in Southeastern Spain I: spectral optical depth, Atmos. Environ., 40, 6453–6464, 2006a.
Lyamani, H., Olmo, F. J., Alcantara, A., and Alados-Arboledas, L.: Atmospheric aerosols during the 2003 heat wave in Southeastern Spain II: microphysical columnar properties and radiative forcing, Atmos. Environ., 40, 6465–6476, 2006b.
Lyamani, H., Olmo, F. J., and Alados-Arboledas, L.: Light scattering and absorption properties of aerosol particles in the urban environment of Granada, Spain, Atmos. Environ., 42, 2630–2642, 2008.
Lyamani, H., Olmo, F. J., and Alados-Arboledas, L.: Physical and optical properties of aerosols over an urban location in Spain: seasonal and diurnal variability, Atmos. Chem. Phys., 10, 239–254, doi:10.5194/acp-10-239-2010, 2010.
Mogo, S., Cachorro, V. E., Sorribas, M., De Frutos, A., and Fernandez, R.: Measurements of continuous spectra of atmospheric absorption coefficients from UV to NIR via optical method, Geophys. Res. Lett., 32, L13811, doi:10.1029/2005GL022938, 2005.
Mona, L., Amodeo, A., Pandolfi, M., and Pappalardo, G.: Saharan dust intrusions in the Mediterranean area: three years of Raman lidar measurements, J. Geophys. Res., 111, D16203, doi:10.1029/2005JD006569, 2006.
Müller, D., Mattis, I., Wandinger, U., Althausen, D., Ansmann, A., Dubovik, O., Eckhardt, S., and Stohl, A.: Saharan dust over a Central European EARLINET–AERONET site: combined observations with Raman lidar and Sun photometer, J. Geophys. Res., 108, 4345, doi:10.1029/2002JD002918, 2003.
Müller, D., Ansmann, A., Mattis, I., Tesche, M., Wandinger, U., Althausen, D., and Pisani, G.: Aerosol-type-dependent lidar ratios observed with Raman lidar, J. Geophys. Res., 112, D16202, doi:10.1029/2006JD008292, 2007.
Müller, D., Heinold, B., Tesche, M., Tegen, I., Althausen, D., Alados-Arboledas, L., Amiridis, V., Amodeo, A., Ansmann, A., Balis, D., Comeron, A., D'amico, G., Gerasopoulos, E., Guerrero-Rascado, J.-L., Freudenthaler, V., Giannakaki, E., Heese, B., Iarlori, M., Knippertz, P., Mamouri, R. E., Mona, L., Papayannis, A., Pappalardo, G., Perrone, R.-M., Pisani, G., Rizi, V., Sicard, M., Spinelli, N., Tafuro, A., and Wiegner, M.: EARLINET observations of the 14–22 May long-range dust transport event during SAMUM 2006: validation of results

from dust transport modeling, Tellus, 61B, 325–339, 2009.
Müller, D., Weinzierl, B., Petzold, A., Kandler, K., Ansmann, A., Müller, T., Tesche, M., Freudenthaler, V., Esselborn, M., Heese, B., Althausen, D., Schladitz, A., Otto, S., and Knippertz, P.: Mineral dust observed with AERONET sun photometer, Raman lidar, and in situ instruments during SAMUM 2006: shape-dependent particle properties, J. Geophys. Res., 115, D11207, doi:10.1029/2009JD012523, 2010.
Omar, A. H., Winker, D. M., Kittaka, C., Vaughan, M. A., Liu, Z., Hu, Y., Trepte, C. R., Rogers, R. R., Ferrare, R. A., Lee, K.-P., Kuehn, R. E., and Hostetler, C. A.: The CALIPSO automated aerosol classification and lidar ratio selection algorithm, J. Atmos. Ocean. Tech., 26(10), 1994–2014, 2009.
Papayannis, A., Amiridis, V., Mona, L., Tsaknakis, G., Balis, D., Bösenberg, J., Chaikovski, A., De Tomasi, F., Grigorov, I., Mattis, I., Mitev, V., Müller, D., Nickovic, S., Perez, C., Pietruczuk, A., Pisani, G., Ravetta, F., Rizi, V., Sicard, M., Trickl, T., Wiegner, M., Gerding, M., Mamouri, R. E., D'Amico, G., and Pappalardo, G.: Systematic lidar observations of Saharan dust over Europe in the frame of EARLINET (2000–2002), J. Geophys. Res., 113, D10204, doi:10.1029/2007JD009028, 2008.
Pappalardo, G., Wandinger, U., Mona, L., Hiebsch, A., Mattis, I., Amodeo, A., Ansmann, A., Seifert, P., Linné, H., Apituley, A., Alados-Arboledas, L., Balis, D., Chaikovsky, A., D'Amico, G., De Tomasi, F., Freudenthaler, V., Giannakaki, E., Giunta, A., Grigorov, I., Iarlori, M., Madonna, F., Mamouri, R.-E., Nasti, L., Papayannis, A., Pietruczuk, A., Pujadas, M., Rizi, V., Rocadenbosch, F., Russo, F., Schnell, F., Spinelli, N., Wang, X., and Wiegner, M.: EARLINET correlative measurements for CALIPSO: first intercomparison results, J. Geophys. Res., 115, D00H19, doi:10.1029/2009JD012147, 2010.
Pereira, S., Wagner, F., and Silva, A. M.: Scattering properties and mass concentration of local and long-range transported aerosols over the South Western Iberia Peninsula, Atmos. Environ., 42, 7623–7631, 2008.
Perez, C., Nickovic, S., Baldasano, J. M., Sicard, M., Rocadenbosch, F., and Cachorro, V. E.: A long Saharan dust event over the western Mediterranean: lidar, Sun photometer observations, and regional dust modeling, J. Geophys. Res., 111, D15214, doi:10.1029/2005JD006579, 2006.
Prats, N., Cachorro, V. E., Sorribas, M., Mogo, S., Berjon, A., Toledano, C., de Frutos, A., de la Rosa, J., Laulainen, N., and de la Morena, B.: Columnar aerosol optical properties during "El Arenosillo 2004 summer campaign", Atmos. Environ., 42, 2643–2653,

doi:10.1016/j.atmosenv.2007.07.041, 2008.
Prospero, J. M.: Long-range transport of mineral dust in the global atmosphere: impact of African dust on the environment of the Southeastern US, P. Natl. Acad. Sci. USA, 96, 3396–3403, 1999.
Prospero, J. M., Ginoux, P., Torres, O., Nicholson, S., and Gill, T.: Environmental characterization of global sources of atmospheric soil dust identified with the NIMBUS7 Total Ozone Mapping Spectrometer (TOMS) absorbing aerosol product, Rev. Geophys., 4(1), 1002, doi:10.1029/2000RG000095, 2002.
Querol, X., Alastuey, A., Moreno, T., Viana, M. M., Castillo, S., Pey, J., Rodriguez, S., Artinano, B., Salvador, P., Sanchez, M., Dos Santos, S. G., Garraleta, M. D. H., Fernandez-Patier, R., Moreno-Grau, S., Negral, L., Minguillon, M. C., Monfort, E., Sanz, M. J., Palomo-Marin, R., Pinilla-Gil, E., Cuevas, E., de la Rosa, J., and de la Campa, A. S.: Spatial and temporal variations in airborne particulate matter (PM_{10} and $PM_{2.5}$) across Spain 1999–2005, Atmos. Environ., 42, 3964–3979, 2008.
Sasano, Y. and Nakane, H.: Significance of the extinction/backscatter ratio and the boundary value term in the solution for the two-component lidar equation, Appl. Optics, 23, 11–13, 1984.
Sasano, Y., Browell, E. V., and Ismail, S.: Error caused by using a constant extinction/backscattering ratio in lidar solution, Appl. Optics, 24, 3929–3932, 1985.
Sicard, M., Molero, F., Guerrero-Rascado, J. L., Pedros, R., Exposito, F. J., Cordoba-Jabonero, C., Bolarin, J. M., Comeron, A., Rocadenbosch, F., Pujadas, M., Alados-Arboledas, L., Martinez-Lozano, J. A., Diaz, J. P., Gil, M., Requena, A., Navas-Guzman, F., and Moreno, J. M.: Aerosol lidar intercomparison in the framework of SPALINET – the SPAnish LIdar NETwork: methodology and results, IEEE T. Geosci. Remote, 47(10), 3547–3559, 2009.
Sioutas, C., Abt, E., Wolfson, J. M., and Koutrakis, P.: Evaluation of the measurement performance of the Scanning Mobility Particle Sizer and Aerodynamic Particle Sizer, Aerosol Sci. Tech., 30, 84–92, 1999.
Sorribas, M.: Medida y Caracterización del Aerosol Atmosférico en un Ambiente Rural y Costero del Suroeste de Europa. La distribución Numérica de Tamaños en el Rango Submicrométrico (Measurements and characterization of atmospheric aerosol in a rural and coastal environment. Sub-micron particle number size distribution in Southwestern Europe), Ph. D. dissertation, University of Valladolid, Valladolid, Spain, 350 pp., available at:

http://sites.google.com/site/marsorribas/, 2008.
Stohl, A.: Computation, accuracy and applications of trajectories – a review and bibliography, Atmos. Environ., 32, 947–966, 1998.
Tesche, M., Ansmann, A., Müller, D., Althausen, D., Mattis, I., Heese, B., Freudenthaler, V., Wiegner, M., Esselborn, M., Pisani, G., and Knippertz, P.: Vertical profiling of Saharan dust with Raman lidars and airborne HSRL in Southern Morocco during SAMUM, Tellus, 61B, 144–164, 2009.
Toledano, C., Cachorro, V. E., de Frutos, A. M., Sorribas, M., Prats, N., and de la Morena, B. A.: Inventory of African desert dust events over the Southwestern Iberian Peninsula in 2000–2005 with an AERONET Cimel Sun photometer, J. Geophys. Res., 112, D21201, doi:10.1029/2006JD008307, 2007a.
Toledano, C., Cachorro, V. E., Berjon, A., De Frutos, A. M., Sorribas, M., De la Morena, B. A., and Goloub, P.: Aerosol optical depth and Angström exponent climatology at El Arenosillo AERONET site (Huelva, Spain), Q. J. Roy. Meteor. Soc., 133, 795–807, 2007b.
Toledano, C., Cachorro, V. E., De Frutos, A. M., Torres, B., Berjon, A., Sorribas, M., and Stone, R. S.: Airmass classification and analysis of aerosol types at El Arenosillo (Spain), J. Appl. Meteorol. Clim., 48(5), 48962–48981, 2009.
Tomasi, F., Blanco, A., and Perrone, M. R.: Raman lidar monitoring of extinction and backscattering of African dust layers and dust characterization, Appl. Optics, 42, 1699–1709, 2003.
Wang, H.-C. and Walter, J.: Particle density correction for the Aerodynamic Particle Sizer, Aerosol Sci. Tech., 6(2), 191–198, 1987.
Welton, E. J., Voss, K. J., Quinn, P. K., Flatau, P. J., Markowicz, K., Campbell, J. R., Spinhirne, J. D., Gordon, H. R., and Johnson, J. E.: Measurements of aerosol vertical profiles and optical properties during INDOEX 1999 using micropulse lidars, J. Geophys. Res., 107(D19), 8019, 18-1–18-20, 2002.
Willeke, K. and Baron, P. A.: Aerosol measurements principles, techniques and applications, Van Nostrand Reinhold, New York, USA, 143–195, 1993.
White, W. H., Macias, E. S., Nininger, R. C., and Schorran, D.: Size-resolved measurements of light scattering by ambient particles in the Southwestern USA, Atmos. Environ., 28, 909–921, 1994.
WMO: GAW Aerosol Measurement Procedures Guidelines and Recommendations, (WMO TD No. 1178) – GAW Report No. 153, World Meteorological Organization, Geneva, 2003.

Zender, C. S., Miller, R., and Tegen, I.: Quantifying mineral dust mass budgets: terminology, constraints, and current estimates, Eos T. Am. Geohpys. Un., 85(48), 509–512, doi:10.1029/2004EO480002, 2004.

Zerefos, C. S., Kourtidis, K. A., Melas, D., Balis, D., Zanis, P., Katsaros, L., Mantis, H. T., Repapis, C., Isaksen, I., Sundet, J., Herman, J., Bhartia, P. K., and Calpini, B.: Photochemical activity and solar ultraviolet radiation modulation factors (PAUR): an overview of the project, J. Geophys. Res., 107(D18), 8134, doi:10.1029/2000JD000134, 2002.

Table 1. Main characteristics of the three lidars used in this study.

	MPL-3	MPL-4	GRA lidar
Station	SCO (28.5° N 16.2° W, 52 m a.s.l.)	ARN (37.0° N 6.7° W, 40 m a.s.l.)	GRA (37.2° N 3.6° W, 680 m a.s.l.)
Routine operation	Yes	No, temporal installation	Yes
Networks	MPLNET SPALINET	– –	EARLINET SPALINET
Wavelength (nm)	523	527	532 (used in this study)
Energy/pulse (mJ)	0.007 (max.)	0.010 (max.)	65
Pulse repetition frequency (Hz)	2500	2500	10
Eye-safe	Yes	Yes	No
Raman capability	No	No	Yes

Table 2. AERONET daily mean AOD^{500}, $AE^{440/675}$ and $LR^{AERONET}$ (see text for details) for the overall dust tracking monitored period (ND denotes no data available).

Site	Santa Cruz de Tenerife (SCO-AEMET)			"El Arenosillo" (ARN-INTA)			Granada (GRA-UGR)		
Day of March 2008	AOD	AE	LR (sr)	AOD	AE	LR (sr)	AOD	AE	LR (sr)
11	0.12±0.01	0.7±0.1	40±8	0.05±0.01	1.0±0.1	46±6	0.09±0.01	1.8±0.3	59±5
12	ND	ND	ND	0.06±0.01	1.3±0.3	45±5	0.09±0.05	1.9±0.3	51±10
13	0.48±0.11	0.3±0.1	50±0	0.08±0.01	1.1±0.3	ND	0.10±0.03	1.1±0.3	ND
14	0.42±0.03	0.4±0.0	59±4	0.41±0.02	0.2±0.0	57±0	0.60±0.28	0.3±0.2	48±3
15	0.28±0.03	0.3±0.0	60±7	0.09±0.02	1.0±0.3	43±12	0.12±0.01	1.6±0.0	76±17
16	0.32±0.03	0.3±0.0	48±6	ND	ND	ND	0.08±0.03	1.7±0.1	57±13
17	0.26±0.04	0.7±0.1	32±4	ND	ND	ND	0.13±0.01	1.1±0.1	ND
18	0.14±0.00	0.7±0.0	ND	0.10±0.01	1.1±0.1	39±1	0.09±0.01	1.9±0.3	55±5
19	0.09±0.01	1.2±0.1	ND	0.07±0.00	0.9±0.0	ND	0.15±0.01	1.8±0.3	ND

Table 3. LR values (at 532 nm) reported by several reference works together with other information for aerosol-type discrimination criteria.

Aerosol type	LR (sr)	AE	Observations	Observational Zone (Campaign)	References
Marine	<40	>1.5	LIDAR	Mediterranean	Balis et al. (2004)[a]
	28±5	0.7±0.4	AERONET		Cattrall et al. (2005)[b]
	23±3		LIDAR	North Atlantic (ACE-2)	Müller et al. (2007)
	20		Satellite (CALIPSO)		Omar et al. (2009)
Mixing (dust/ no-dust particles)	38±10	0.5–1.0	LIDAR	Southern Italy	Tomasi et al. (2003)
	40–60	0.5–1.5	LIDAR	Mediterranean	Balis et al. (2004)[a]
Dust	>60	<0.5	LIDAR	Mediterranean	Balis et al. (2004)[a]
	42±4	0.1±0.1	AERONET		Cattrall et al. (2005)[b]
	55±5	0.2±0.2	LIDAR	Sahara (SAMUM)	Müller et al. (2007)
	59±11	0.5±0.5	LIDAR	Sahara (EARLINET)	Müller et al. (2007)
	40/65 (polluted dust)		Satellite (CALIPSO)		Omar et al. (2009)

[a] At 355 nm
[b] At 550 nm

Table 4. Date and starting and ending times together with the maximum and minimum TV concentration values as reached for each size range of the DDP episode in both ARN and GRA stations.

TV range	Day Starting time	Day Ending time	TV concentration ($\mu m^3\,cm^{-3}$) Minimum–maximum
ARN station			
TV0	15 Mar 03:00 UTC	15 Mar 09:00 UTC	4.3–8.8
TV1	15 Mar 00:00 UTC	15 Mar 09:00 UTC	1.5–2.3
TV2	15 Mar 00:00 UTC	15 Mar 05:00 UTC	5.3–10.6
TV3	14 Mar 06:00 UTC	14 Mar 03:00 UTC	3.0–11.1
GRA station			
TV0	–	–	–
TV1	14 Mar 14:00 UTC	15 Mar 12:00 UTC	0.7–4.0
TV2	14 Mar 14:00 UTC	15 Mar 12:00 UTC	3.9–13.8
TV3	14 Mar 23:00 UTC	15 Mar 12:00 UTC	10.9–28.6

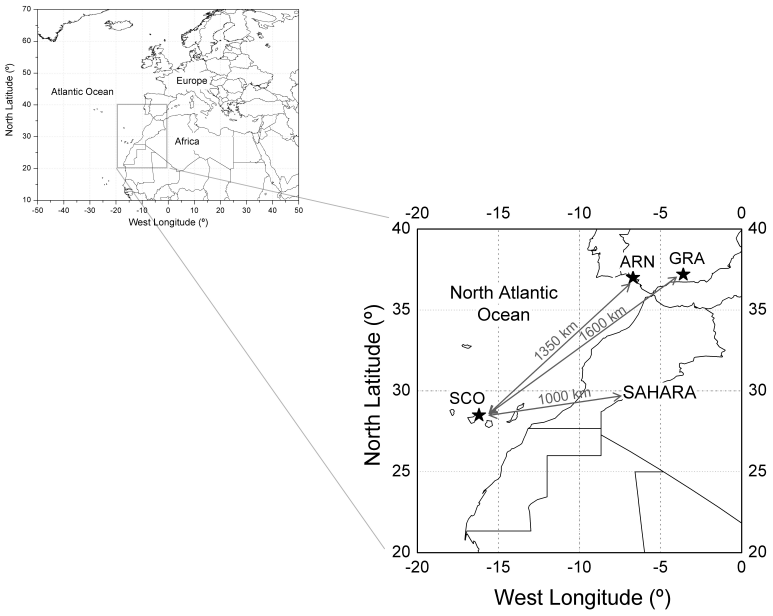

Fig. 1. Map showing the geographical situation of the three stations, Santa Cruz de Tenerife (SCO), "El Arenosillo" (ARN) and Granada (GRA) respect to Saharan dust sources.

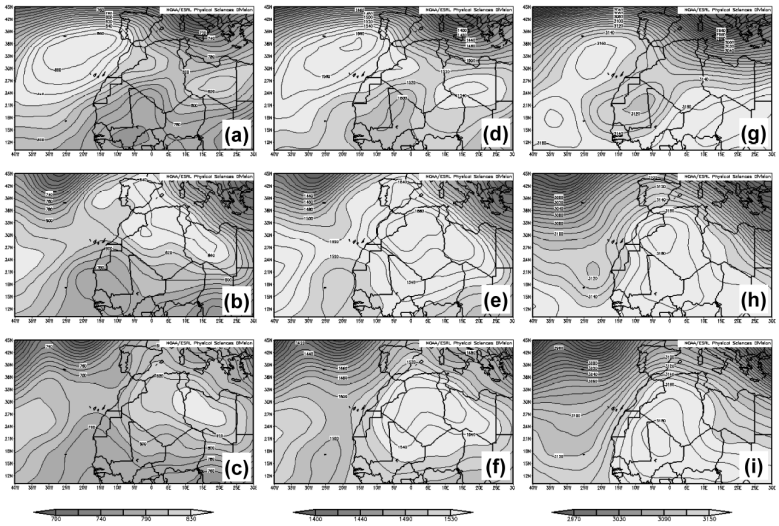

Fig. 2. Meteorological synoptic charts at three geopotential heights: 950 hPa (800 m a.s.l., **a–c**), 850 hPa (1500 m a.s.l., **d–f**) and 700 hPa (around 3000 m a.s.l., **g–i**). Figure panels correspond to three different dates as representative of both no-dusty and dusty conditions depending on each station (from top to bottom panels): 11 March, 13 March and 14 March 2008.

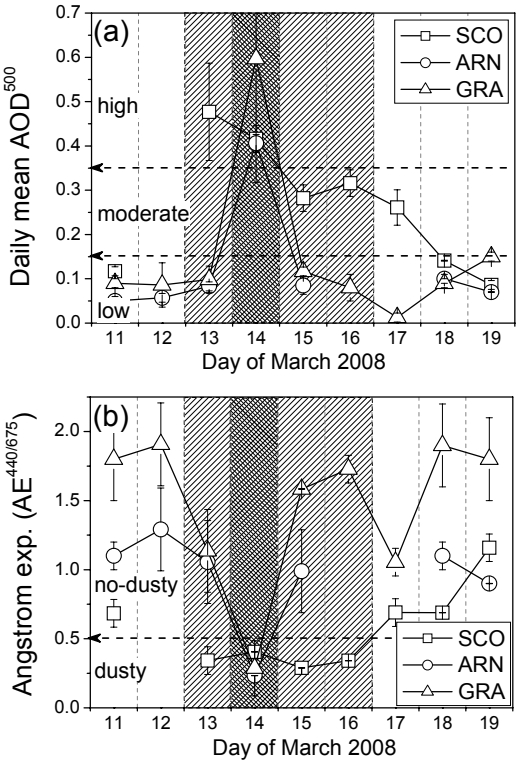

Fig. 3. (a) Daily mean AOD at 500 nm (AOD^{500}) and **(b)** Angstrom exponent ($AE^{440/675}$) for these three stations. Dusty periods are marked by light- and dark-shaded areas over SCO and ARN/GRA sites, respectively.

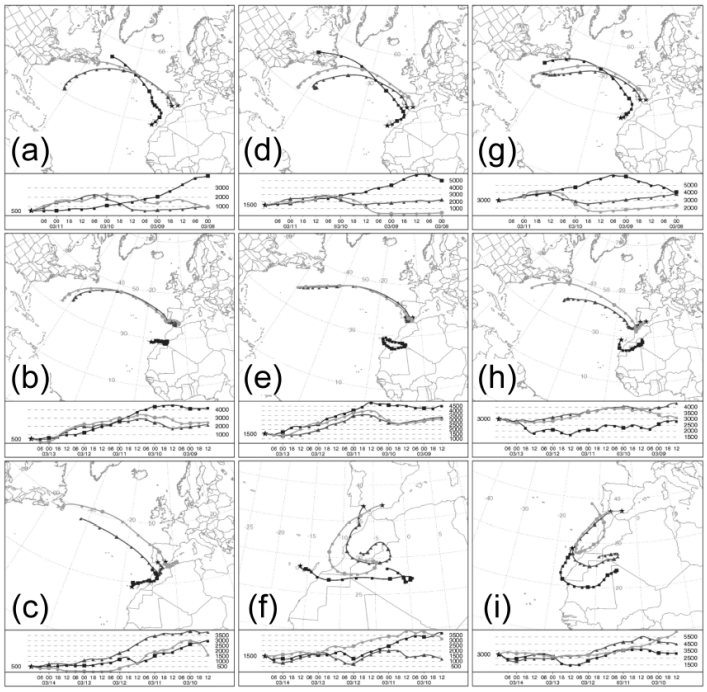

Fig. 4. HYSPLIT 5-day backtrajectories ending at 12:00 UTC over SCO (square line), ARN site (triangle line) and GRA (circle line) sites at different altitudes (a.g.l.): 500 m **(a–c)**, 1500 m **(d–f)** and 3000 m **(g–i)**. Figure panels correspond to three different dates as representative of both no-dusty and dusty conditions depending on each station (from top to bottom panels): 11 March, 13 March and 14 March 2008.

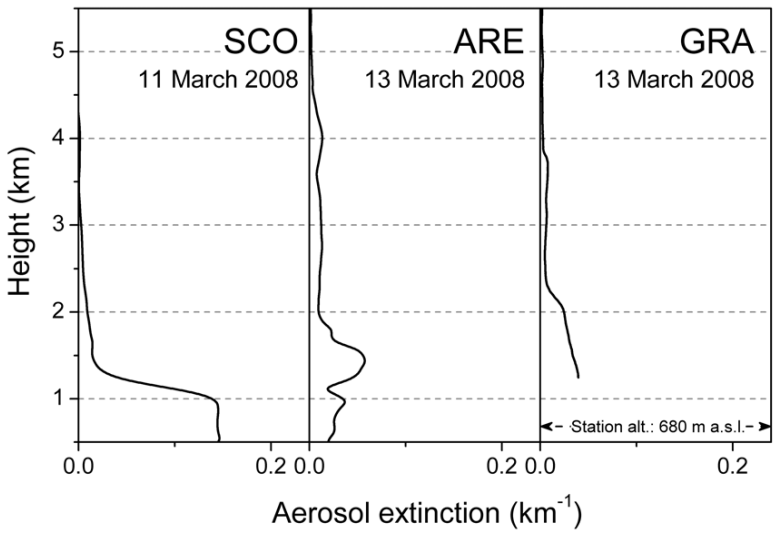

Fig. 5. Height-resolved extinction coefficients at 12:00 UTC (1-h averaged profiles) for no-dusty conditions over SCO site (left), and ARN (centre) and GRA (right) stations (GRA station is placed at 680 m a.s.l.). Date of no-dusty lidar measurements is indicated in each panel.

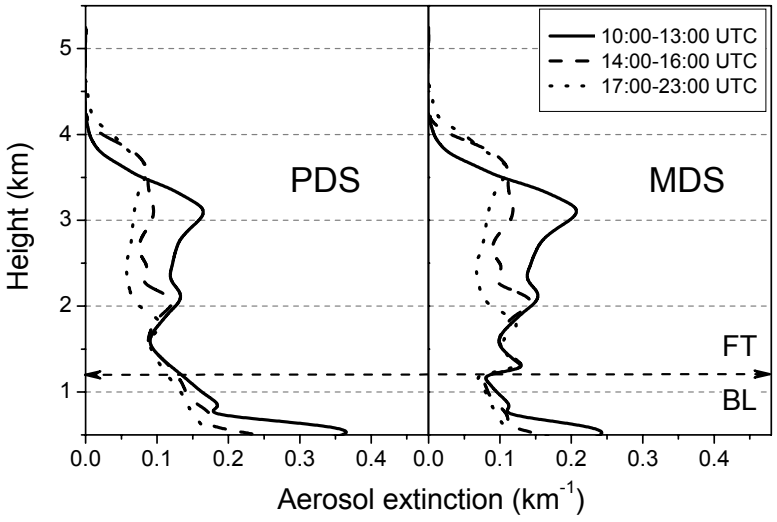

Fig. 6. Height-resolved extinction coefficients under dusty conditions (13 March 2008) over SCO site for both the "pure-dust scenario" (PDS) (left) and the "mixed-dust scenario" (MDS) (right) at selected averaged times (see legend).

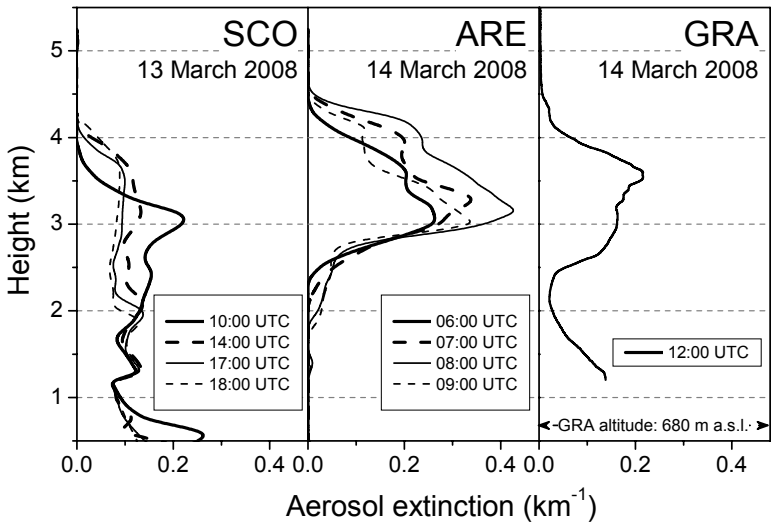

Fig. 7. Height-resolved extinction coefficients (1-h averaged profiles) at discrete times (see legend) under dusty conditions over SCO site (left), ARN (centre) and GRA (right) stations. Date of lidar measurements is indicated in each panel.

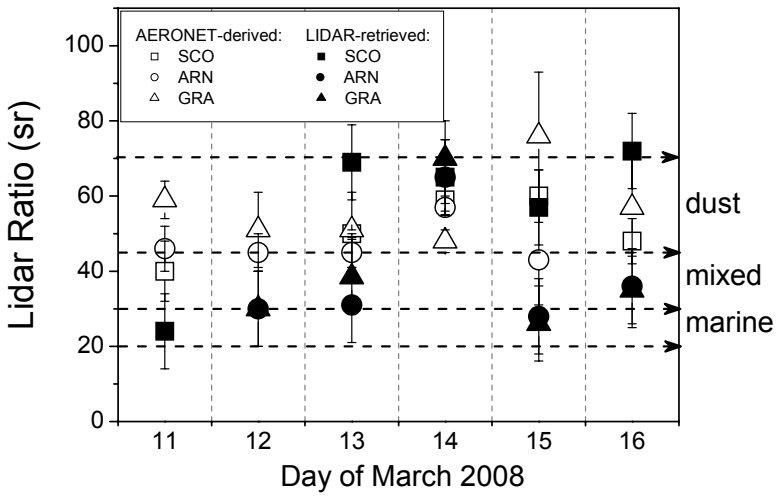

Fig. 8. Lidar-retrieved LR (extinction-to-backscatter ratio) values together with those columnar-integrated AERONET-derived ones (see Table 2). LR ranges adopted for aerosol-type discrimination are also marked (shaded arrows).

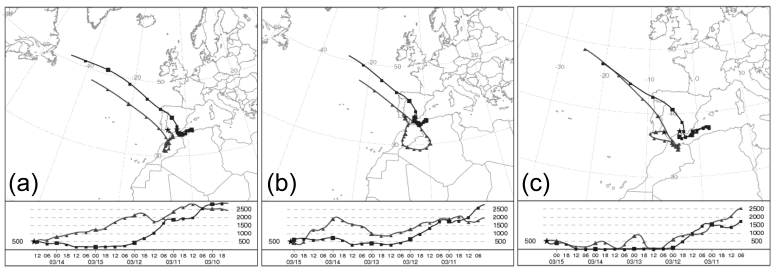

Fig. 9. HYSPLIT 5-day backtrajectories ending at 500 m height a.g.l. over both ARN (triangle line) and GRA (square line) sites. Figure panels correspond to three representative dates and times for that dust episode: 14 March at 14:00 UTC **(a)**, 15 March at 02:00 UTC **(b)** and 15 March at 06:00 UTC **(c)**.

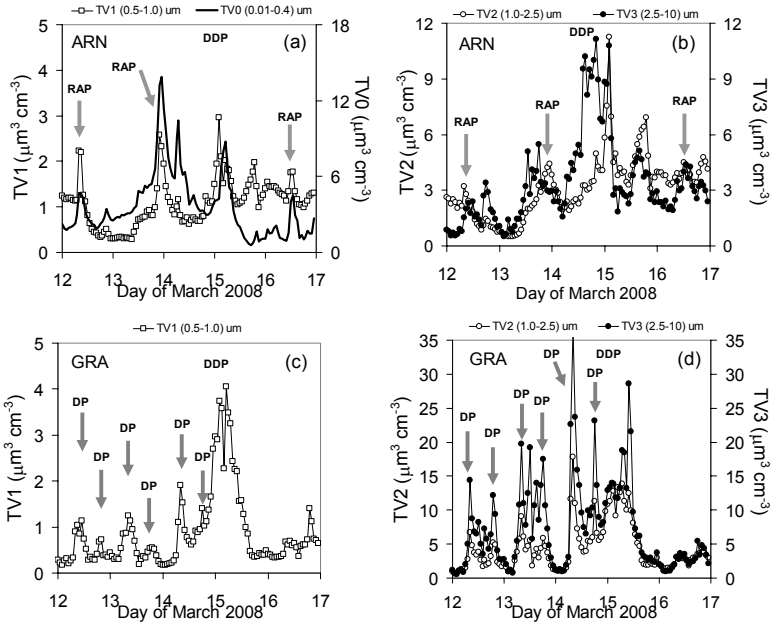

Fig. 10. Temporal evolution of the total volume (TV) particle concentration (hourly integrated) for four discrete size ranges: 0.01–0.4 μm (TV0), 0.5–1.0 μm (TV1), 1.0–2.5 μm (TV2) and 2.5–10.0 μm (TV3) for the overall period of 12–16 March 2008, in both ARN (**a** and **b**) and GRA (**c** and **d**) sites. Selected aerosol episodes are marked by grey arrows (Regional Anthropogenic Plume, RAP, and Diurnal Pattern, DP) and shaded area (Desert Dust Plume, DDP) in each case.

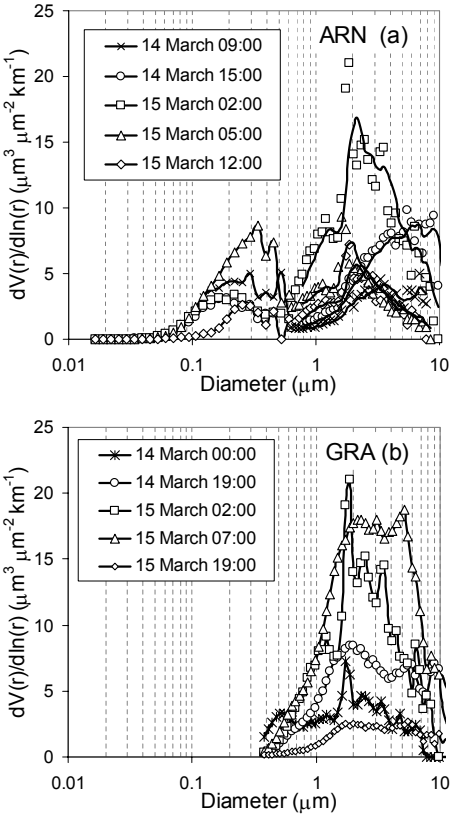

Fig. 11. Selected in time volume size distributions (VSD) at ground level in both ARN **(a)** and GRA **(b)** sites.

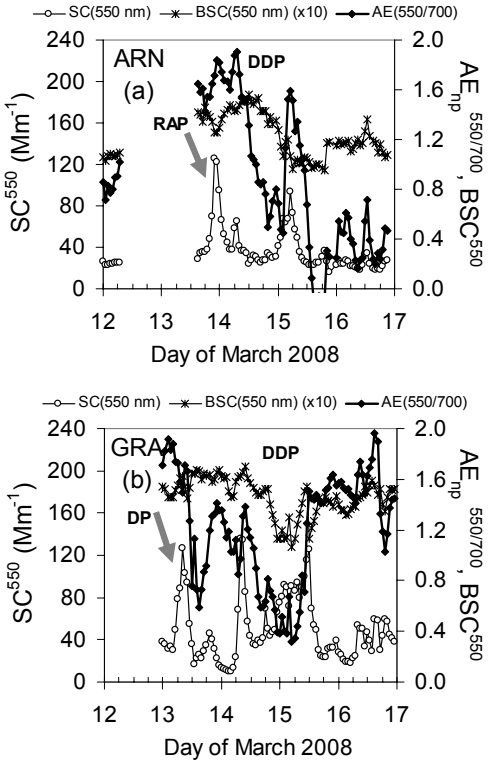

Fig. 12. Temporal evolution of the scattering coefficient at 550 nm (SC^{550}), the Angstrom Exponent ($AE_{np}^{550/700}$) and the backscatter fraction at 550 nm (BSC^{550}) for surface particles with a particle diameter lower than 10 μm for the overall period of 12–16 March 2008 in both **(a)** ARN and **(b)** GRA sites.

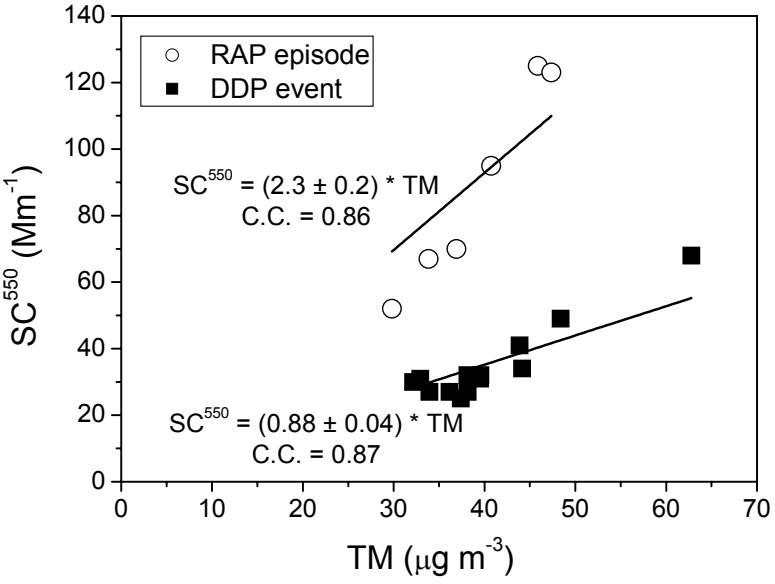

Fig. 13. Relation between SC550 y total mass (TM) concentration (as evaluated from the volume size distribution and assuming a particle density of 2 g cm^{-3}), during a Regional Anthropogenic Plume (RAP) episode and the Desert Dust Plume (DDP) event over ARN station.